J. Nonlinear Sci. Vol. 11: pp. 123–168 (2001)
DOI: 10.1007/s00332-001-0002-y

Journal of
Nonlinear
Science

Nonlinear Propagation of Light in One-Dimensional Periodic Structures

R. H. Goodman,[1,2] M. I. Weinstein,[1] and P. J. Holmes[2,3]

[1] Mathematical Sciences Research, Fundamental Mathematics Department, Bell Laboratories–Lucent Technologies, 600 Mountain Avenue, Murray Hill, NJ 07974, USA
e-mail:goodmanr@research.bell-labs.com
e-mail:miw@research.bell-labs.com

[2] Program in Applied and Computational Mathematics, Princeton University, Princeton, NJ 08544, USA

[3] Department of Mechanical and Aerospace Engineering, Princeton University, Princeton, NJ 08544, USA
e-mail:pholmes@rimbaud.princeton.edu

Received September 13, 2000; accepted February 2, 2001
Communicated by Gerard Iooss

Summary. We consider the nonlinear propagation of light in an optical fiber waveguide as modeled by the anharmonic Maxwell-Lorentz equations (AMLE). The waveguide is assumed to have an index of refraction that varies periodically along its length. The wavelength of light is selected to be in resonance with the periodic structure (Bragg resonance). The AMLE system considered incorporates the effects of noninstantaneous response of the medium to the electromagnetic field (chromatic or material dispersion), the periodic structure (photonic band dispersion), and nonlinearity. We present a detailed discussion of the role of these effects individually and in concert. We derive the nonlinear coupled mode equations (NLCME) that govern the envelope of the coupled backward and forward components of the electromagnetic field. We prove the validity of the NLCME description and give explicit estimates for the deviation of the approximation given by NLCME from the *exact* dynamics, governed by AMLE. NLCME is known to have gap soliton states. A consequence of our results is the existence of very long-lived gap soliton states of AMLE. We present numerical simulations that validate as well as illustrate the limits of the theory. Finally, we verify that the assumptions of our model apply to the parameter regimes explored in recent physical experiments in which gap solitons were observed.

1. Introduction

There is a great deal of current interest in nonlinear optical phenomena in periodic structures. This interest has been fueled by advances in fabrication methods for periodic

media and in their potential for use as components in all-optical communication systems and computers. The potential for applications is due to the rich variety of phenomena that result from the interactions of sufficiently intense (nonlinear) electromagnetic fields with the underlying (linear) dispersion characteristics of the periodic structure [47]. The reason one may envision the use of nonlinear periodic structures in optical devices stems from the observation that one can achieve very strong dispersion of a light pulse over very short distances by arranging the wavelength of light and period of the medium to be appropriately resonant. At sufficiently high intensities, one then expects a balance between nonlinear and dispersive effects over short distances, thus giving rise to a rich class of phenomena in structures of small physical dimensions.

This paper is motivated by experiments and theory on nonlinear wave propagation in one-dimensional periodic structures. Our goal is to validate the nonlinear coupled mode equations (NLCME), a model commonly used to describe this situation, and to clarify the roles played by the various physical mechanisms. The experiments involve the propagation of intense light in an optical fiber waveguide whose core has a periodically varying index of refraction along the length of the fiber, a *fiber grating* [25]. Experimentalists have observed the formation of *gap solitons*, solitary-wave–like localized structures whose time-frequency parameters lie in the photonic band-gap associated with the background periodic structure. These are of potential interest for use in all optical storage devices, since they can, in principle, travel at arbitrarily low speeds. Theoretical work on nonlinear propagation in periodic structures goes back to work of Winful et al. [44], [45], and Chen and Mills [8]. Explicit gap soliton solutions were derived in the context of a slowly varying envelope theory by Christodoulides and Joseph [9] and in a more general form by Aceves and Wabnitz [1]. For surveys on aspects related to this paper, see de Sterke and Sipe [11], Brown and Eggleton [7], and Kurizki et al. [17]. Experiments demonstrating the existence of gap solitons have been performed by Eggleton, Slusher, and collaborators [13], [14], [15], and by Broderick and his collaborators [6], [34]. In two and three dimensions, Aközbek and John have formally derived envelope equations and examined their solitary waves numerically [3].

In the remainder of this section, we give a brief overview of the underlying physics and modeling assumptions. We also introduce the analytical and numerical results developed in this article.

Electromagnetic wave propagation in a dielectric medium is described by Maxwell's equations together with an appropriate constitutive relation describing how electromagnetic waves interact with matter. An optical fiber has a high index *core* and a slightly lower index *cladding*. This index configuration confines rays to the core (total internal reflection) or, from the wave perspective, the index profile provides a potential well with a ground state (core mode) having most of its energy confined to the core. In the regimes that interest us here, to a very good approximation the energy distribution has a fixed transverse structure given by the core mode, and one may think of the transverse core mode amplitude as varying with time t and distance along the waveguide, z. In addition to this geometric constraint, we incorporate the following effects:

(i) *Noninstantaneous response of the medium to the field*: The polarization, P, is related to the electric field, E, via an anharmonic Lorentz oscillator model.

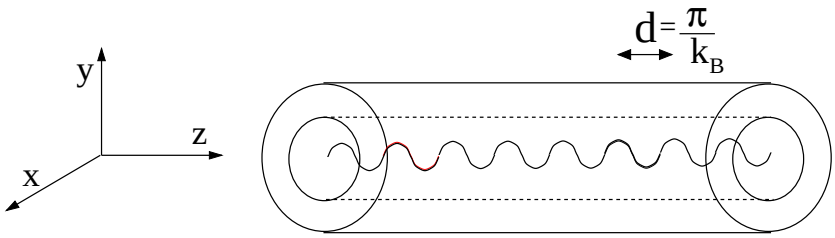

Fig. 1. A schematic drawing of an optical fiber with periodic refractive index variation.

(ii) *Periodicity of the medium*: Spatial periodicity of the medium is built in by allowing the coefficients of the anharmonic Lorentz oscillator to vary periodically in space. A schematic of the physical system is shown in Figure 1.
(iii) *Nonlinear effects at appropriate intensities*: The implied relation between P and E is such that regions of higher intensity $|E|^2$ have higher refractive index. This is a so-called focusing (Kerr) nonlinearity. The localized region of higher intensity effectively creates an attractive potential well.

The effects of noninstantaneous response and spatial periodicity each give rise to *dispersion*, the property that waves of different wavelengths travel at different speeds. The type of dispersion due to (i) is called *chromatic or material dispersion* and that arising due to effect (ii) is called *photonic band dispersion*. This results from interference effects arising from reflection and transmission in the periodic structure.

A model incorporating the above geometric constraints and physical effects is a variant of the Anharmonic Maxwell-Lorentz system [5], [36], [24], which incorporates the spatial periodicity. This system is displayed in (6), and we shall refer to it below as AMLE.[1]

While in a bare (homogeneous, nongrated) optical fiber, light injected at one end of the waveguide will propagate with little back-scatter, significant back-scattering will occur in the presence of a periodic refractive index. This effect is most pronounced when the wavelength of light is roughly twice the grating period, $2d$, the case of *Bragg resonance*. In this case there is strong coupling between backward and forward waves. We will assume that the variation of the index of refraction about its mean is small and is denoted by a parameter ε. In terms of this parameter, we consider the following scaling regime:

- amplitude of the field $\sim \mathcal{O}(\sqrt{\varepsilon})$, and
- initial spectral support of the pulse is concentrated in a wavenumber range of width $\mathcal{O}(\varepsilon)$ about $\pm k_B \equiv \pm\pi/d$.

Therefore, the spatial structure of the fields E and P may be viewed as functions of the form $\sqrt{\varepsilon}A(\varepsilon x)e^{ik_B x}$, where $A(y)$ is a localized function of y. We shall refer to this as

[1] In the nonlinear optics literature, the relation between polarization P and electric field E is often taken to have the form: $P = \int_{-\infty}^{t} \chi(t-\tau)E(\tau)d\tau + \cdots$. The class of models we have chosen gives the same envelope equation, NLCME, in the scaling regime considered but has the added feature that it conserves energy. Energy estimates are central to our proof of the validity of NLCME: Theorem 1.

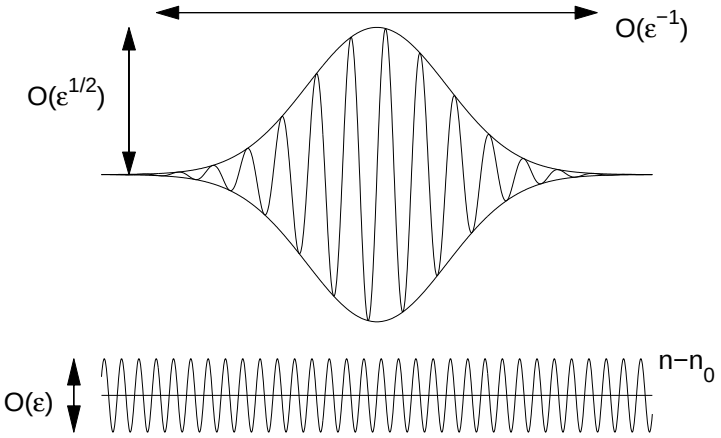

Fig. 2. A schematic of a wave packet under the SVEA, with envelope with width ε^{-1}, amplitude $\sqrt{\varepsilon}$, carrier wavelength $2d$, and a plot of the index of refraction variation with variation of size ε and period d.

the *slowly varying envelope approximation* (SVEA). A schematic of this scaling ansatz is shown in Figure 2.

Under these assumptions, *nonlinear coupled mode equations* (NLCME, see equations 10) can be derived that govern the forward E_+ and backward E_- propagating electric field wave envelopes on timescales of order ε^{-1}. Thus, in this regime, the fine scale grating oscillations are effectively averaged and the original mathematical description in terms of a nonlinear partial differential equation with spatially periodic coefficients is replaced by a constant coefficient dispersive nonlinear partial differential equation.

The main results of this paper are as follows:

Characterization of Phenomena: The formation of long-lived coherent structures (gap solitons) is the result of a balance between the effects of dispersion and nonlinearity.[2] The energy in a wave packet, with frequency content localized about the Bragg resonant frequency, resolves into backward and forward propagating waves. If the field amplitude is appropriately large relative to the the amplitude of periodic variations in the medium, then wave energy does not disperse and is localized in space. Nonlinearity generates ever higher harmonics which is manifested in wave steepening and apparent carrier shock formation; see Sections 3.4 and 3.6. However, in the presence of material dispersion due to finite time response, a stable balance between dispersion and nonlinearity is achieved; no shocks form, and one has long-lived stable gap solitons (see Section 2.2, Theorem 1, and the corollary of Section 3.7). We also verify (Appendix A)

[2] In contrast to the case of bare fiber, for which this balance is achieved over lengths of optical fiber on the order of tens of kilometers, for the periodic structures and intensities used in the above cited experiments, this balance occurs on a length scale of centimeters; see Appendix B.

that parameter ranges corresponding to experiments are described by our model and theorem.

Analytical—Theorem 1: We prove that solutions to the initial value problem for AMLE with finite energy and nearly monochromatic initial conditions, as above, give rise to solutions that are well-approximated, on appropriate timescales ($\mathcal{O}(\varepsilon^{-1})$) by a superposition of amplitude-modulated backward and forward propagating plane waves. The backward and forward amplitudes satisfy NLCME. Further, we estimate the deviation of the NLCME approximation to the AMLE solution. An important class of solutions of NLCME are so-called *gap solitons*.[3] These are spatially localized nonlinear bound states [1] that have been observed experimentally. Our results imply the existence of gap soliton wave packets for AMLE on timescales $\mathcal{O}(\varepsilon^{-1})$, see Section 6. Our method follows previous rigorous studies of the validity of solutions to envelope equations in approximating oscillatory, nearly monochromatic solutions to evolution PDEs in one space dimension; see, for example, Kirrman, Schneider, and Mielke [27] and Pierce and Wayne [37]. A related method presented in the context of dissipative equations is given by van Harten [41]. Important extensions of such methods have been developed in Donnat and Rauch [12], Joly, Metivier, and Rauch [23], Lannes [31], and Schochet [39], [40] where multidimensional and multiphase problems are treated. These papers do not treat the resonant interactions of multiphase waves with periodic media, although the formulation of [12], e.g., can easily be extended to deal with the present one-space-dimensional problem. Here, however, we provide a self-contained, elementary treatment of the one-dimensional problem. We also wish to note a recent general paper of Babin and Figotin [4] on wave interactions in periodic media.

Numerical Simulations: We numerically simulate AMLE and NLCME and systematically compare their computer-generated solutions with a view toward checking the error estimates of Theorem 1. Initial data appropriate for Theorem 1 consists of a slow modulation of a highly oscillatory wave. In the main numerical example presented in Section 7, we have simulated the AMLE evolution with gap soliton wave packet initial data. We take data with an envelope whose full width at half maximum (FWHM) measured in wavelengths of light is about 60; see Figure 7. In one run, the simulation of AMLE took about $2\frac{1}{2}$ hours, while the corresponding simulation of NLCME took only a few minutes on a 500 mHz Pentium III computer running Linux. The advantage is even larger when wavepackets with more oscillations are investigated. For parameter regimes of physical interest, it is probably infeasible to simulate the full AMLE, while it is quite simple to simulate the NLCME. In the physical experiments [13], pulses on the the order of 30 ps FWHM are observed, $\mathcal{O}(10^4)$ wavelengths.

In our numerical simulations, we identify three time regimes. The first is the timescale on which the coherent structure evolves as a gap soliton plus fluctuations satisfying the

[3] Here, we adopt a common usage of the term *soliton* as referring to a nonlinear bound state solution or solitary wave. The term originally and still often refers more specifically to nonlinear bound states arising in completely integrable systems.

estimates of Theorem 1. The second is a longer timescale on which the wave envelope predicted by NLCME gives an accurate prediction of where the field energy is, but due to phase drift, the norm estimates of the error in Theorem 1 fail to hold. The third is a regime on which the wave envelope begins to steepen asymmetrically and radiate energy, leading to a decay of the gap soliton. A description of this process would require the inclusion of higher order nonlinear wave-steepening and dispersive corrections to NLCME.

The structure of this paper is as follows:

In Section 2.1 we introduce the anharmonic Maxwell-Lorentz model (AMLE) and in Section 2.2 we describe and display the nonlinear coupled mode equations, discuss their mathematical structure, and state our main theorem (Theorem 1) relating solutions of AMLE to those of NLCME. In Section 3 we discuss the effect of the nonlinearity, periodic structure, and material dispersion and describe the physical effects of including, excluding, and variously combining these mathematical features of the system. In Section 4 we present a derivation of NLCME from AMLE using the method of multiple scales, and in Section 5 we discuss existence and uniqueness results for AMLE and NLCME, some of which are needed in Section 6, where we prove Theorem 1. In Section 7 we report on numerical simulations and careful systematic comparison of solutions to AMLE and NLCME. In Section 8 we present a short summary followed by a discussion of issues meriting further investigation. The appendices contain a discussion of nondimensionalization and physical parameter magnitudes, and details of dimensionless values used in the numerical simulations.

Notation and Conventions

Throughout this paper, we make use of following notation:

The symbols C, C_j are used to represent generic constants whose dependence on parameters is specified when of concern.

For a vector-valued function $\vec{f}(z)$, the L^p-norm is given by

$$\|\vec{f}\|_p = \left(\int \sum_j |f_j(z)|^p dz \right)^{1/p}. \tag{1}$$

Here and throughout, spatial (z) integrals are taken over $-\infty < z < \infty$. The space L^p is then the space of all functions $\vec{f}$ such that $\|\vec{f}\|_p$ is finite.

The L^∞ norm is given by

$$\|\vec{f}\|_\infty = \max_j \left(\operatorname{ess\,sup} |f_j(z)| \right), \tag{2}$$

with the space L^∞ thus defined as the set of all (essentially) bounded functions.

The H^s norms may be defined as

$$\|\vec{f}\|_{H^s}^2 = \sum_{k=1}^{s} \left\| \frac{d^k}{dx^k} \vec{f} \right\|_2^2. \tag{3}$$

The space H^s is the space of all functions $\vec{f}$ such that $\|\vec{f}\|_{H^s}$ is finite, that is, the space of functions such that the function and its first s derivatives are square-integrable.

Finally, for a given Banach space X, with norm $\|\cdot\|_X$, we define

$$C([0,T);X)$$

to be the set of functions $f\colon t \mapsto f(t) \in X$ that are continuous for $t \in [0,T)$ with values in X.

2. The AMLE and NLCME Equations

2.1. AMLE, Nondimensionalization, and Parameter Regimes

In this subsection we introduce AMLE with physical parameters and then introduce its nondimensional form. We then discuss parameter regimes associated with the above mentioned experiments.

We take as our basic model a one-dimensional electromagnetic system satisfying Maxwell's equation, with the polarization governed by an anharmonic Lorentz oscillator model,[4] henceforth referred to as the anharmonic Maxwell-Lorentz equations (AMLE) [5], [24], [36],

$$\mu_0 \partial_t D = \partial_t B, \;\; \partial_t B = \partial_z E, \tag{4a}$$

$$D \equiv \epsilon_0 E + P, \tag{4b}$$

$$\tilde{\omega}_0^{-2} \partial_t^2 P + \left(1 - 2\Delta n \cos(2\tilde{k}_B z)\right) P - \tilde{\phi} P^3 = \epsilon_0 \chi^{(1)} E. \tag{4c}$$

Here, E is the electric field, B is the magnetic field, P is the polarization, and D is the electric displacement. ϵ_0 and μ_0 denote, respectively, the permitivity and permeability of free space, and $\chi^{(1)}$ is the linear polarizability of the medium. Recall that $\epsilon_0 \mu_0 = c^{-2}$, where c is the vacuum speed of light. Δn measures the strength of the grating. We shall also write

$$\Delta n = \varepsilon \nu, \tag{5}$$

where ε measures the size of the index modulation and ν is of order one and is introduced in order to make explicit how the spatially periodic structure rears its head in the envelope approximation, NLCME, to be derived below.

---

[4] Our results and analysis apply to the generalization of this model where we take P to be a weighted sum of N polarizations, P_i, corresponding to different molecular excitation modes of the material:

$$P = \sum_{i=1}^{N} P_i; \qquad \tilde{\omega}_i^{-2} \partial_t^2 P_i + (1 - 2\Delta n_i \cos(2\tilde{k}_B z)) P_i - \tilde{\phi}_i P_i^3 = \epsilon_0 \chi_i^{(1)} E.$$

This model can be viewed as a nonlinear generalization of the Sellmeier model (132); see [2]. With this particular modeling of the polarization, AMLE has the important property of being an energy conserving system. This structure gives rise to *energy estimates* that are central to our proofs of well-posedness of AMLE and of the validity of NLCME as an approximating envelope equation; see Sections 5 and 6.

The spatial period of the medium is d and is expressed in terms of

$$\tilde{k}_B = \frac{\pi}{d}.$$

Since we are interested in the propagation of light with wavelength equal to the Bragg wavelength, we set

$$\lambda = 2d,$$

where d denotes the period of the grating.

In Appendix A, we eliminate the magnetic field B from this system and nondimensionalize these equations. There, nondimensional dependent variables are primed, but here we drop primes for simplicity of notation. From (127), (125b), and (125c), we obtain

$$\partial_t^2 D = \partial_z^2 E, \tag{6a}$$

$$D \equiv E + P, \tag{6b}$$

$$\omega_0^{-2}\partial_t^2 P + (1 - 2\varepsilon\nu\cos(2k_B z))P - \phi P^3 = (n^2 - 1)E. \tag{6c}$$

ω_0 is a dimensionless frequency, and ϕ is a dimensionless measure of the degree of the nonlinearity. The limit of instantaneous polarization is achieved by taking the parameter $\omega_0 \to \infty$. This gives the relation

$$P = P(E) = (1 + 2\varepsilon\nu\cos(2k_B z))E + \chi^{(3)}E^3 + \cdots,$$

with nonlinear polarizability $\chi^{(3)}$ and, in this case, equation (6) reduces to the scalar nonlinear wave equation,

$$\partial_t^2(n^2 E + 2\varepsilon\nu\cos(2k_B z)E + \chi^{(3)}E^3) = \partial_z^2 E. \tag{7}$$

2.2. NLCME and Main Results

The nonlinear coupled mode equations are introduced by considering slow modulations to solutions of the anharmonic oscillator model in which the photonic structure and nonlinearity are ignored. When $\varepsilon = 0$ and $\phi = 0$, system (6) supports plane wave solutions of the form $E = E_\pm e^{i(\pm kz - \omega t)}$, where $k = k(\omega)$ is the dispersion relation (see Section 3) and $E_\pm$ are constants. A similar statement holds for P. In the scaling regime described in the introduction, in which nonlinear effects and spatial periodicity are allowed, and where the carrier wave has wavenumber k_B and frequency $\omega_B = \omega(k_B)$, we seek coupled and *slowly modulated* backward and forward plane wave solutions of the form

$$\begin{pmatrix} E^\varepsilon_{NLCME} \\ P^\varepsilon_{NLCME} \end{pmatrix} \sim \sqrt{\varepsilon}\left(E_+(Z,T)e^{i(k_B z - \omega_B t)} + E_-(Z,T)e^{-i(k_B z + \omega_B t)} + c.c.\right)\begin{pmatrix} 1 \\ \gamma_B \end{pmatrix} \tag{8}$$

where $c.c.$ denotes the complex conjugate of the previous expression and $\gamma_B = \gamma(\omega_B)$ is a constant. Here, Z and T are "slow variables,"

$$Z = \varepsilon z, \qquad T = \varepsilon t, \tag{9}$$

and E_+ and E_- satisfy equations of the form[5]

$$i\left(\partial_T E_+ + v_g \partial_Z E_+\right) + \kappa E_- + \Gamma(|E_+|^2 + 2|E_-|^2)E_+ = 0, \tag{10a}$$

$$i\left(\partial_T E_- - v_g \partial_Z E_-\right) + \kappa E_+ + \Gamma(|E_-|^2 + 2|E_+|^2)E_- = 0. \tag{10b}$$

Here, κ is a coupling parameter (proportional to ν induced by the grating), v_g is the group velocity of the linear dispersive wave at frequency ω_B, and Γ is the nonlinear coupling parameter (proportional to ϕ). The explicit expressions for these coefficients are displayed in Section 4, during the derivation of (10); see (61).

The expression in (8) for E^ε and P^ε is a formal approximate solution to AMLE satisfying the "nearly monochromatic" initial condition:

$$\begin{pmatrix} E(z, t=0) \\ P(z, t=0) \end{pmatrix} = \sqrt{\varepsilon}\left(E_{0+}(\varepsilon z)\vec{v}_+ e^{ikz} + E_{0-}(\varepsilon z)\vec{v}_- e^{-ikz} + c.c.\right) + \mathcal{O}(\varepsilon), \tag{11}$$

where $\vec{v}_\pm$ are constant two-component vectors.

We prove the following result in Section 6:

Theorem 1. *Consider AMLE with a general nonlinearity satisfying Hypothesis 2 of Section 6. There exists $\varepsilon_0 > 0$ such that for any $T_0 > 0$ and any $0 < \varepsilon \leq \varepsilon_0$, the solution $\begin{pmatrix} E^\varepsilon_{AMLE} \\ P^\varepsilon_{AMLE} \end{pmatrix}$ of AMLE with data (11) belonging to H^3 is well approximated by a solution of NLCME in the sense that for all $t \in [0, T_0/\varepsilon]$ the following estimate holds:*

$$\left\| \begin{pmatrix} E^\varepsilon_{AMLE} \\ P^\varepsilon_{AMLE} \end{pmatrix} - \begin{pmatrix} E^\varepsilon_{NLCME} \\ P^\varepsilon_{NLCME} \end{pmatrix} \right\|_{H^1} \leq C(T_0; \omega_0, \nu, n)\varepsilon. \tag{12}$$

We note that due to Sobolev's inequality, $|f(x)| \leq C\|f\|_{H^1}$, a small error in the H^1 norm ensures a small pointwise error, so that the above statement gives uniform bounds on the error.

3. AMLE, NLCME, and Physical Phenomena

The physical phenomena modeled by AMLE and NLCME result from competition among: (i) nonlinear effects, (ii) dispersion due to finite time response of the medium to the field, and (iii) dispersion due to reflection and transmission in a spatially periodic medium. This section is divided into subsections in which we study, by considering

[5] Beginning with a three-dimensional Maxwell-Lorentz model in fiber geometry, it is possible to derive similar nonlinear coupled mode equations, with one difference being that the term $\Gamma(|E_\pm|^2 + 2|E_\mp|^2)E_\pm$ is replaced by one of the form $(\Gamma_s|E_\pm|^2 + 2\Gamma_\times|E_\mp|^2)E_\pm$, where Γ_s and $\Gamma_\times$ are the nonlinear self-phase modulation and cross-phase modulation coefficients, and depend on certain integrals of the transverse modes of the waveguide [1], [35]. Another difference one finds is that the transverse potential, defined by the refractive index profile, induces *waveguide or modal dispersion*. Thus, a more complete description of the physics leads to corrections to the free space dispersion relation due to material dispersion, photonic band dispersion, and modal dispersion, as well. The multidimensional analyses of [12], [23], [31], [40], [39], which assume "almost" plane wave solutions, do not appear to generalize (easily) to the waveguide problem.

various choices of ω_0, ε, and ϕ in (6), the action of these effects (terms in the equations) individually and in concert.

3.1. Linear Spatially Homogeneous Structure with Instantaneous Response

In this case, $\varepsilon = \phi = 0$ and $\omega_0 = \infty$. Therefore, $P = (n^2 - 1)E$ and the evolution is described by the classical wave equation,

$$n^2 \partial_t^2 E = \partial_z^2 E, \tag{13}$$

whose solutions are of the form

$$E(z, t) = e_+(z - t/n) + e_-(z + t/n), \tag{14}$$

corresponding to a a superposition of left and right moving waves that propagate without distortion.

Alternatively, we can first seek elementary plane wave solutions $E(z, t; k) = e^{-i\omega t + ikx}$. We then find that ω and k are related by the simple *dispersion relation* $\omega(k) = \pm\frac{k}{n}$. Since the phase velocity, $\omega(k)/k$, is independent of k, all wavelengths travel at the same speed, and we refer to (13) as *nondispersive*. Standard Fourier superposition of these plane waves yields the general solution (14).

3.2. Linear and Homogeneous Medium with Finite Time Response

In this case, we have

$$\partial_t^2 (E + P) = \partial_z^2 E, \tag{15a}$$

$$\omega_0^{-2} \partial_t^2 P + P = (n^2 - 1)E. \tag{15b}$$

We may still find plane wave solutions

$$\begin{pmatrix} E_0 \\ P_0 \end{pmatrix} = \begin{pmatrix} 1 \\ \gamma \end{pmatrix} e^{i(kz - \omega t)}, \tag{16}$$

where k and ω are related by the *dispersion relation*

$$k^2 = \omega^2 \frac{n^2 - \left(\frac{\omega}{\omega_0}\right)^2}{1 - \left(\frac{\omega}{\omega_0}\right)^2}, \tag{17}$$

and

$$\gamma = \frac{n^2 - 1}{1 - \left(\frac{\omega}{\omega_0}\right)^2}. \tag{18}$$

In the relevant parameter regimes, $\omega_0^2 > \omega^2$ and $n^2 - 1 > 0$. So, γ is positive, corresponding to polarization in phase with the electric field. Note that in the $\omega_0 \to \infty$ limit, we recover the wave equation dispersion relation $k = \pm\omega n$.

A general solution may be constructed by superposition of these plane waves using the Fourier Transform. Using the method of stationary phase [43], one can show that for initial data whose Fourier transform decays sufficiently rapidly, the amplitude of the solution decays as $t^{-\frac{1}{2}}$.

3.3. Linear Periodic Structure, Instantaneous Response

In this case, we take $\phi = 0$ and $\varepsilon \neq 0$. We consider the case of instantaneous response, $\omega_0 = \infty$, though the methods apply to finite ω_0 as well. In this case we have the scalar one-dimensional wave equation with spatially periodic wave speed:

$$\left(n^2 + 2\varepsilon(n^2 - 1)\nu\cos(2k_B z)\right)\partial_t^2 E = \partial_z^2 E. \tag{19}$$

In analogy with the scalar and spatially homogeneous wave equation, we seek solutions of the form $E(z,t) = e^{-i\omega t}\varphi(z)$. This yields the Mathieu equation:

$$-\partial_z^2\varphi(z) = \omega^2\left(n^2 + 2\varepsilon(n^2 - 1)\nu\cos(2k_B z)\right)\varphi(z). \tag{20}$$

We now seek solutions of (20) of the form

$$\varphi(z) = e^{iKz}\psi(z;K), \qquad K \in [0, 2\pi), \tag{21}$$

$$\psi(z + d; K) = \psi(z;K), \tag{22}$$

where ψ has the same periodicity as the medium. Therefore, $\psi(z;K)$ satisfies the boundary value problem:

$$-(\partial_z + iK)^2\psi(z;K) = \omega^2\left(n^2 + 2\varepsilon(n^2 - 1)\nu\cos(2k_B z)\right)\psi(z;K), \tag{23}$$

$$\psi(z + d; K) = \psi(z;K), \qquad d \equiv \frac{\pi}{k_B}. \tag{24}$$

For each K, there is a discrete set of eigen-solutions $\{\varphi_m(z;K) : m = 1, 2, \ldots\}$ with corresponding eigenvalues $\{\omega_m(K)^2 : m = 1, 2, \ldots\}$. As K varies over the interval $[0, 2\pi)$, the functions $\omega_m^2(K)$ sweep out spectral (photonic) bands. These bands are separated by spectral (photonic band) gaps. The solutions

$$E_m(z,t;K) = e^{-i\omega_m(K)t + iKz}\psi_m(z;K), \quad K \in [0, 2\pi), \quad m = 1, 2, \ldots. \tag{25}$$

are generalizations of plane wave solutions of the previous subsections. In contrast to the homogeneous medium case, where the allowable set of frequencies varies over the entire real line, in the periodic case the allowable set of frequencies varies over selected bands. The band dispersion relations, $\{\omega_m(K) : m = 1, 2, \ldots\}$, play the role of the dispersion relation, $\omega(K)$, for the homogeneous medium (constant coefficient partial differential equation). Since the phase velocities $\omega_m(K)/K$ are not independent of K, we see that wave propagation in periodic media is dispersive. A generalization of Fourier superposition holds, enabling one to construct the general solution to the initial value problem for (19). A careful stationary phase analysis of this superposition formula can be made, yielding results on the spreading and temporal decay of solutions [30].

Thus, Floquet-Bloch theory gives a complete characterization of wave propagation in a linear periodic medium. However, the key to understanding the detailed properties of this propagation is a detailed knowledge of the band dispersion functions, $\omega_m(K)$. This is a difficult problem, in general. In the case when the periodicity is given by a small oscillation about its mean (ε small), *coupled mode theory* [29] can be used to approximate the Floquet-Bloch spectral theory. This provides a satisfactory description of the wave propagation for large, but finite, times. We illustrate this for equation (19). The idea is that for ε small, the solutions $E_m(z, t; K)$ should be well-approximated by plane waves of the unperturbed $\varepsilon = 0$ problem. Thus, we seek solutions of (19) in the form

$$E = \left(E_+(\varepsilon z, \varepsilon t)e^{ik_B(z-t/n)} + E_-(\varepsilon z, \varepsilon t)e^{-ik_B(z+t/n)} + c.c.\right) + \mathcal{O}(\varepsilon), \tag{26}$$

and derive equations for the slowly varying functions $E_+(Z, T)$, $E_-(Z, T)$, ensuring that (26) is a good approximation of a solution for times, t, of order ε^{-1}. This approximation and error estimates are derived systematically in Sections 4 and 6 in the nonlinear context of AMLE. In this linear setting, the equations reduce to the *linear coupled mode equations* (*cf.* equations (10)):

$$i\left(\partial_T E_+ + v_g \partial_Z E_+\right) + \kappa E_- = 0, \tag{27a}$$

$$i\left(\partial_T E_- - v_g \partial_Z E_-\right) + \kappa E_+ = 0, \tag{27b}$$

where $v_g \equiv \omega' = n^{-1}$ is the group velocity (which happens to agree here with the phase velocity, $\omega(k)/k$), and $\kappa = \frac{k(n^2-1)v}{2n}$.

The opening of the first "photonic band gap" can be deduced from (27). Seeking solutions to (27) of the form

$$\begin{pmatrix} E_+ \\ E_- \end{pmatrix} = e^{i(QZ-\Omega(Q)T)} \begin{pmatrix} \mathcal{E}_+ \\ \mathcal{E}_- \end{pmatrix}, \tag{28}$$

we find

$$\Omega^2(Q) = n^{-2}Q^2 + \kappa^2. \tag{29}$$

The photonic band gap is pictured in Figure 3, which clearly shows a region of excluded frequencies centered around $\Omega = 0$. For Ω in the gap, Q is imaginary, indicating that frequencies in Bragg resonance with the grating cannot propagate.

Finally, combining (28) and (29) with (26) gives the following approximation to a *band edge* Floquet-Bloch generalized plane wave:

$$\begin{aligned} &E(z, t; K)|_{K=k_B+\varepsilon Q} \\ &\quad = \mathcal{E}_+ e^{i[(k_B-\varepsilon Q)z-(\omega_B+\varepsilon\Omega(Q))t]} + \mathcal{E}_- e^{-i[(k_B+\varepsilon Q)z+(\omega_B+\varepsilon\Omega(Q))t]} + \mathcal{O}(\varepsilon). \end{aligned} \tag{30}$$

3.4. Nonlinearity, Instantaneous Response, and No Periodic Structure

Here, we take $\omega_0 \to \infty$ and $\varepsilon = 0$ in (6). The equations then reduce to

$$\partial_t^2(E + P) = \partial_z^2 E, \tag{31a}$$

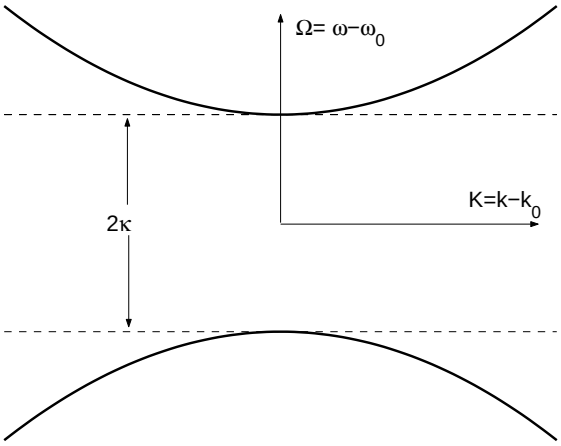

Fig. 3. The dispersion relation for the linearized coupled mode equations, showing the spectral gap.

and, for small E,

$$P = P(E) = (n^2 - 1)E + \chi^{(3)}E^3 + \cdots. \tag{31b}$$

These may be combined to give

$$\partial_t^2 D(E) = \partial_z^2 E, \tag{32a}$$

$$D(E) = n^2 E + \chi^{(3)}E^3 + \cdots. \tag{32b}$$

To study this system, we first rewrite it in a more standard form. Let $v \equiv \mathcal{K}^{-1}(E) \equiv D(E)$. Then, (32a) becomes $\partial_t^2 v = \partial_z^2 \mathcal{K}(v)$. Introducing $\partial_z u = v$, we obtain after one integration

$$\partial_t^2 u = \partial_z \mathcal{K}(\partial_z u). \tag{33}$$

Equation (33) has the form of the equation governing the vibrations of a nonlinear string, where the electric displacement, $D(E)$, plays the role of the strain, $\partial_z u$.[6]

A classical result of Lax [32] states that systems which are *genuinely nonlinear* in the sense that $\mathcal{K}''(0) \neq 0$, or equivalently $D''(0) \neq 0$, will develop singularities in finite time. Since $D''(0) = 0$, the quasilinear (32a) does not satisfy the genuine nonlinearity condition, although $D'''(0) \neq 0$. Klainerman and Majda [28] generalized Lax's result; if $\partial_E^{(p+1)} D(0) \neq 0$ and the initial data is of size ε, then singularity formation takes place within a time interval of length $\mathcal{O}(\varepsilon^{-p})$.

In particular, it follows from this result that for initial data of size $\mathcal{O}(\sqrt{\varepsilon})$ (see (8)), $u(z,t)$ develops a singularity in its second derivatives within $\mathcal{O}(\varepsilon^{-1})$ time. Thus, E

[6] The classical relation between tension, τ, and strain, $\partial_z u$, is derived via

$$\mathcal{K}(\partial_z u) = \partial_z u(1 + (\partial_z u)^2)^{-\frac{1}{2}}\tau(\partial_z u).$$

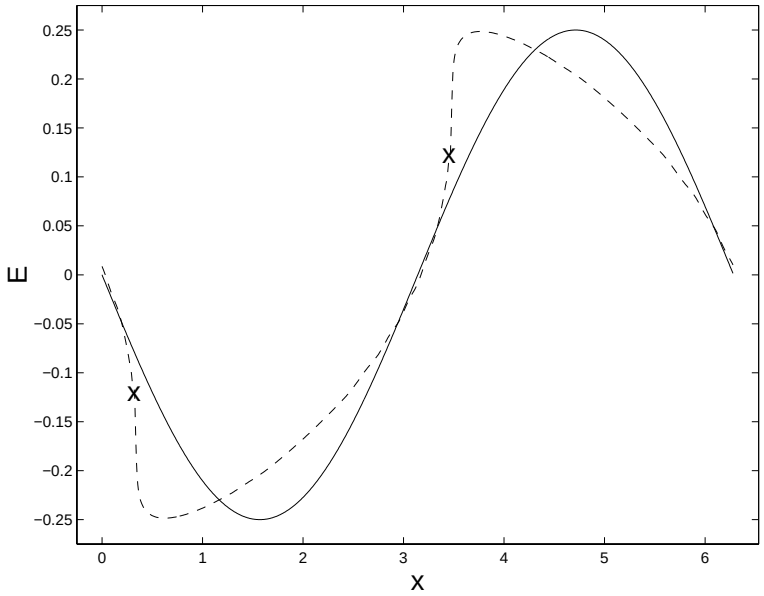

Fig. 4. Evolution from sinusoidal initial conditions (solid line) to near shock formation (dashed line, with shock location at the **x**) in Maxwell's equation with instantaneous nonlinear polarization.

remains bounded, but $\partial_z E$ tends to infinity at the singularity time. This is a *shock* type singularity. Specifically, the results of [28] imply the following:

Theorem 2. *Consider the quasilinear wave equation (32a) with smooth initial data* $E(z, t = 0)$, $\partial_t E(z, t = 0)$, *which are of order* $\sqrt{\varepsilon}$. *Then, there exists a finite and positive time,* $T(\varepsilon) \leq C\varepsilon^{-1}$, *such that*

$$\sup_{0\leq t\leq T(\varepsilon)} \|E(\cdot, t)\|_\infty < \infty, \tag{34}$$

while

$$\lim_{t\nearrow T(\varepsilon)} \|\partial_z E(\cdot, t)\|_\infty + \|\partial_t E(\cdot, t)\|_\infty = \infty. \tag{35}$$

Such carrier shock formation in the context of nonlinear optics has been discussed by heuristic arguments in [16], [19].

Figure 4 shows a simulation of the shocking process on a single carrier wave.[7] Computational details are given in Section 7, and computational parameters for this and all subsequent numerical results are given in Appendix C.

[7] This computation is actually performed on the AMLE system with a very fast material response $\omega_0 \gg 1$; see Appendix C. The simulation is run to the time the shock "would have formed" in the absence of material dispersion.

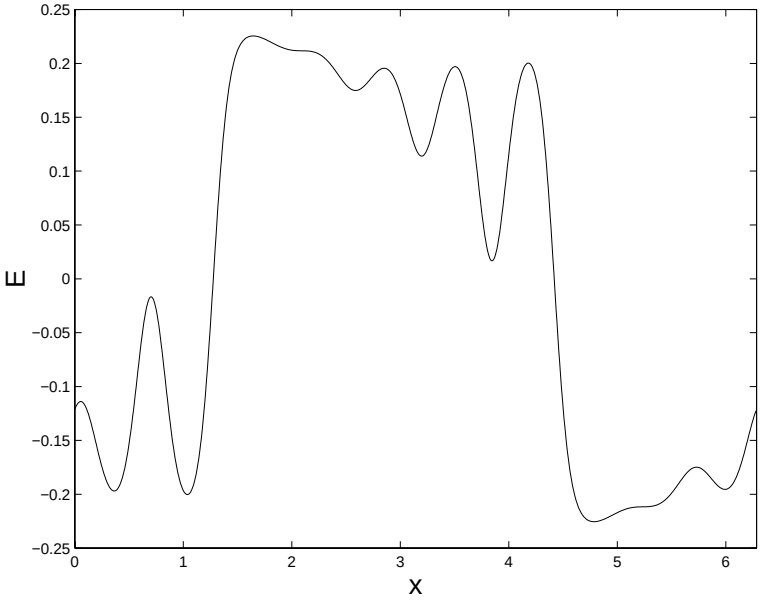

Fig. 5. Solution of AMLE after the "shock time" with small ω_0.

3.5. Nonlinearity, Finite Time Response, and No Periodic Structure

The mathematical model in this case is AMLE, (6) with $\varepsilon = 0$. Joly, Metivier, and Rauch [24] proved that the initial value problem for the full three-dimensional AMLE, for some class of nonlinearities, does not develop singularities in finite time. In Section 5 we outline a proof of this result for our simpler one-dimensional model. Therefore, material dispersion, resulting from the finite response time ($\omega_0 < \infty$), inhibits shock formation by providing a mechanism for expelling high frequency modes away from the steepening regions.

Numerical experiments suggest an interesting small dispersion limit as ω_0 tends to infinity in (6c). Note that for $0 < \omega_0 < \infty$ the system is semilinear, but the limiting system is quasi-linear.

Two computations with increasing values of ω_0 are shown in Figures 5 and 6 at a short time after the shock formation time in the dispersionless ($\omega_0 = \infty$) limit. As $\omega_0 \to \infty$, the number of oscillations increases and, in some weak sense, the solution more closely approximates a weak solution to the Maxwell system with instantaneous nonlinear polarization.

The small material dispersion ($\omega_0 \gg 1$) limit of AMLE is analogous to the small dispersion limit of the Korteweg-de Vries equation (KdV),

$$\partial_t u + u\partial_z u + \varepsilon \partial_z^3 u = 0, \tag{36}$$

the equation of the free surface of an air/water interface in the regime of long waves of small amplitude. The dispersionless $\varepsilon = 0$ equation is the *inviscid Burgers equation* and is easily seen to develop shocks (singularities in derivatives of u) in finite time [43]. For $\varepsilon \neq$

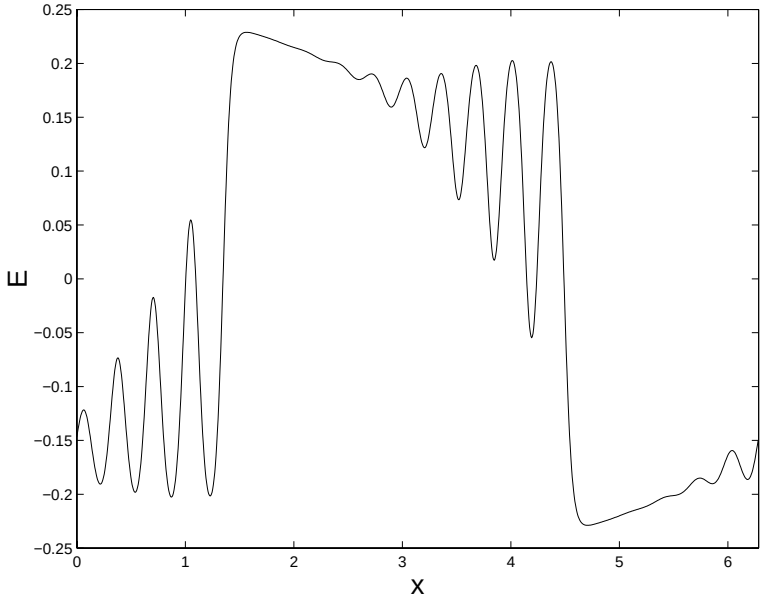

Fig. 6. Solution of AMLE after the "shock time" with ω_0 twice that of Figure 5.

0, solutions of KdV do not develop singularities [26]. For initial data that give rise to shock formation for $\varepsilon = 0$, one observes, for ε small, a scenario analogous to what we observe for AMLE in the limit of ω_0 large. KdV is an integrable Hamiltonian system that is exactly solvable using the inverse scattering transform (IST) [18]. IST was used by Lax and Levermore [33] and by Venakides [42] to study this small dispersion limit. In particular, the generation of oscillations is related to the dynamics of solitons. As in the case of KdV, for AMLE one observes the generation of solitary-wave–like oscillations as a result of carrier wave steepening. Computer simulations indicate that these solitary waves interact more strongly and generate radiation, a manifestation of AMLE's apparent nonintegrability.

3.6. Periodic Structure with Nonlinearity, Instantaneous Response

In this case, the electric field is governed by

$$\partial_t^2 D(E, z) = \partial_z^2 E, \tag{37a}$$

$$D(E, z) = \left(n^2 + 2\varepsilon\nu\cos(2k_B z)\right) E + \phi E^3. \tag{37b}$$

The multiple scales approach implemented in Section 4 formally yields an expansion of the form (compare with (8))

$$E = \sqrt{\varepsilon}\sum_{m\geq 1}\left(E_+^{(m)}(Z, T)e^{imk_B(z-t/n)} + E_-^{(m)}(Z, T)e^{-imk_B(z+t/n)}\right) + c.c. + \varepsilon^{\frac{3}{2}}E_1, \tag{38}$$

where $E_\pm^{(m)} = E_\pm^{(m)}(Z, T) \equiv E_\pm^{(m)}(\varepsilon z, \varepsilon t)$, $m \geq 1$, satisfies a coupled system of infinitely many partial differential equations. This is in contrast to the case $\omega_0 < \infty$,

where the expansion is replaced by (8) involving only the *two* amplitudes $E_{\pm}^{(1)}$ at leading ($\mathcal{O}(\sqrt{\varepsilon})$) order.

The reason for this difference can be seen by examining the equation for the correction, E_1, which takes the form

$$\begin{aligned}\left(n^2\partial_t^2 - \partial_z^2\right) E_1 &= \sum_{q\geq 1}[A_q^+(T, Z)e^{iq(kz-\omega(k)t)} + A_q^-(T, Z)e^{iq(kz+\omega(k)t)}] \\ &= \sum_{q\geq 1}[A_q^+(T, Z)e^{iqk(z-t/n)} + A_q^-(T, Z)e^{iqk(z+t/n)}]. \end{aligned} \tag{39}$$

The coefficients $A_q^{\pm}$ involve the unknown amplitudes $E_{\pm}^{(m)}$ and their derivatives. In order for εE_1 to be smaller than the first term in the expansion of E, it is necessary to remove all resonances from the right-hand side. Resonances are excited by components of the right-hand side which are plane waves of the homogeneous problem. If $0 < \omega_0 < \infty$, the unperturbed dynamics are dispersive ($\omega(qk) \neq q\omega(k)$). Therefore, the contributions to the above sum for $q \geq 2$ are nonresonant, and the nonresonance condition implies coupled equations for $E_+^{(1)}$ and $E_-^{(1)}$ alone. In the case of instantaneous response ($\omega_0 = \infty$: absence of material dispersion), all terms in the sum are resonant. Therefore, in order to preclude secular growth, we require $A_m^{\pm} \equiv 0$, $m \geq 1$. This yields a coupled system of *infinitely* many equations governing the evolution of the backward and forward amplitudes: $E_{\pm}^{(m)}(Z, T)$, $m \geq 1$. We do not address the question of whether the approximate solution generated, via (38), is a convergent series that represents an approximate solution of Maxwell's equation.

Indeed, the contrast we find between the dispersive (ω_0 positive and finite) and nondispersive ($\omega_0 = \infty$) cases is consistent with the observations of the previous section concerning shock formation and therefore the generation of high frequency harmonics.[8]

Consequently, the NLCME system does not describe the evolution of the wavepacket envelope for the system without material dispersion. Although the ratio of the effects of photonic band dispersion to material dispersion in the experiments of Eggleton, Slusher, et al. [13], [14], [15] is of order 10^6, we argue that nonlinearity rapidly (on a timescale of order $\tilde{\omega}_0^{-1}$) generates frequency content for which material dispersion is significant; see Appendix B. As noted in Section 3.5, material dispersion regularizes the wave steepening by propagating nonlinearly generated frequencies, which are nearly resonant, away from a steepening front.

3.7. Periodic Structure, Nonlinearity, and Finite Time Response

In this case, we have the full AMLE equations (6). We show in Theorem 1 that, for small amplitude waves in the SVEA regime, solutions to AMLE are well approximated by solutions to the Nonlinear Coupled Mode Equations (NLCME).

[8] Note, however, that the simulations described in the previous section are not for wavepacket initial conditions. It is reasonable to ask whether the dispersion that comes from the photonic band structure is sufficient to regularize shocks. Preliminary direct simulations for the nondispersive ($\omega_0 = \infty$) limit employing numerical schemes designed to capture shock-like structures indicate that shocks very likely form in the carrier, though the *envelope* appears to evolve smoothly (E. Kirr, in progress).

The NLCME have a well-known class of solutions known as "gap solitons," which are able to propagate through the fibers at any velocity between zero and the speed of light. We present them in the general form as derived by Aceves and Wabnitz [1]. The solutions depend on two parameters, $|v| < 1$ and δ,

$$E_+ = s\alpha e^{i\eta}\sqrt{\left|\frac{\kappa}{2\Gamma}\right|}\frac{1}{\Delta}(\sin\delta)\, e^{is\sigma}\,\mathrm{sech}\,(\theta - is\delta/2); \tag{40a}$$

$$E_- = -\alpha e^{i\eta}\sqrt{\left|\frac{\kappa}{2\Gamma}\right|}\Delta(\sin\delta)\, e^{is\sigma}\,\mathrm{sech}\,(\theta + is\delta/2); \tag{40b}$$

where

$$\gamma = \frac{1}{\sqrt{1-v^2}}, \qquad \Delta = \left(\frac{1-v}{1+v}\right)^{\frac{1}{4}},$$
$$\theta = \gamma\kappa(\sin\delta)(v_g^{-1}Z - vT), \qquad \sigma = \gamma\kappa(\cos\delta)(v_g^{-1}vZ - T),$$
$$s = \mathrm{sign}\,(\kappa\Gamma), \qquad \alpha = \sqrt{\frac{2(1-v^2)}{3-v^2}},$$
$$e^{i\eta} = \left(-\frac{e^{2\theta} + e^{-is\delta}}{e^{2\theta} + e^{is\delta}}\right)^{\frac{2v}{3-v^2}}.$$

Combining this family of exact solutions to NLCME with Theorem 1, we have the following corollary:

Corollary 1. *The gap solitons approximate to $\mathcal{O}(\varepsilon)$ a family of long-lived solutions to the AMLE system for times of $\mathcal{O}(\varepsilon^{-1})$.*

The gap solitons solutions bear a striking resemblance to solitons of the Nonlinear Schrödinger equation (NLS). In fact, in the limit $\delta \ll 1$, $v \ll 1$, we may show that the gap soliton may be written as a normal mode of linear coupled mode equations, slowly modulated by an NLS soliton. To see this, we study the NLCME themselves under the SVEA limit. We assume δ small, and look for approximate solutions to (10) of the form

$$\begin{pmatrix} E_+ \\ E_- \end{pmatrix} \approx \delta A(\delta Z, \delta T, \delta^2 T)\vec{V}e^{i(QZ-\Omega T)}, \tag{41}$$

where $\vec{V}e^{i(QZ-\Omega T)}$ solves the linearized NLCME. Then $\Omega_\pm = \pm\sqrt{\kappa^2 + v_g^2Q^2}$, and A solves

$$i\,\partial_\tau A + \frac{\Omega''(Q)}{2}\partial_\zeta^2 A + N|A|^2A, \tag{42}$$

with

$$\zeta = \delta(Z - \Omega'(Q)T), \qquad \tau = \delta^2 T,$$
$$\text{and } N = \frac{\Gamma}{2}\left(3 - \frac{v_g^2Q^2}{\kappa^2 + v_g^2Q^2}\right).$$

NLS has spatially localized standing wave solutions of the form

$$A(\zeta,\tau)=\pm\sqrt{\frac{2\lambda}{N}}e^{i\lambda\tau}\,\mathrm{sech}\left(\sqrt{\frac{2\lambda}{\Omega_+''(Q)}}\zeta\right), \tag{43}$$

and if we let $Q=0$ and $\lambda=\frac{\kappa}{2}$ in this formula, then we recover exactly the leading term in the expansion of the gap soliton for $v=0$ and $\delta\ll 1$. De Sterke and Sipe [11] show additionally that the first two terms in the expansion of the gap soliton for small δ and v correspond to the $\mathcal{O}(\delta)$ and $\mathcal{O}(\delta^2)$ terms in the multiple scales construction of solutions to AMLE with small wavenumber Q.

Therefore, we expect the following relationship among AMLE, NLCME, and NLS. For $\delta<\delta_0$ sufficiently small, NLCME has a solution of the type (41), where $A(\zeta,\tau)$ satisfies NLS. The validity of NLS as an approximation to NLCME could be shown using the methods presented in Section 6 and [27]. This solution of NLCME, generated by NLS, gives rise to a solution of AMLE of the type (8), provided $\varepsilon\le\varepsilon(\delta_0)$ is sufficiently small.

4. Derivation of the Nonlinear Coupled Mode Equations

In this section we use the method of multiple scales [43] to derive the nonlinear coupled mode equations. We begin with the equation

$$\partial_t^2(E+P)=\partial_z^2E. \tag{44a}$$

We also specify a more general form for the nonlinear response in modeling the polarization in (6c),

$$\omega_0^{-2}\partial_t^2P+(1-2\varepsilon\nu\cos(2k_Bz))P+g(P,z)=(n^2-1)E, \tag{44b}$$

where, for small values of P,

$$g(P,z)=-\phi P^3+\text{higher order terms}. \tag{45}$$

We expand the dependent variables in powers of ε,

$$E=\varepsilon^{\frac12}E_0+\varepsilon^{\frac32}E_1+\varepsilon^{\frac52}E_2+\cdots, \tag{46}$$

$$P=\varepsilon^{\frac12}P_0+\varepsilon^{\frac32}P_1+\varepsilon^{\frac52}P_2+\cdots, \tag{47}$$

and expand the derivatives in terms of slow scales $Z=\varepsilon z$ and $T=\varepsilon t$:

$$\partial_t\to\partial_t+\varepsilon\partial_T\quad\text{and}\quad\partial_z\to\partial_z+\varepsilon\partial_Z. \tag{48}$$

To derive the NLCME, it will be sufficient for us to consider the equations for the first two terms in the expansion, which may be written

$$\mathcal{O}(\varepsilon^{1/2}):\ \mathcal{L}_0\begin{pmatrix}E_0\\P_0\end{pmatrix}=0, \tag{49}$$

$$\mathcal{O}(\varepsilon^{3/2}):\ \mathcal{L}_0\begin{pmatrix}E_1\\P_1\end{pmatrix}=-\mathcal{L}_1\begin{pmatrix}E_0\\P_0\end{pmatrix}+\begin{pmatrix}0\\2\nu\cos(2k_Bz)P_0+\phi P_0^3\end{pmatrix}, \tag{50}$$

where

$$\mathcal{L}_0 = \mathcal{L}_0(i^{-1}\partial_t, i^{-1}\partial_z) = \begin{pmatrix} \partial_t^2 - \partial_z^2 & \partial_t^2 \\ 1 - n^2 & 1 + \omega_0^{-2}\partial_t^2 \end{pmatrix}, \tag{51}$$

and

$$\mathcal{L}_1 = 2\begin{pmatrix} \partial_t\partial_T - \partial_z\partial_Z & \partial_t\partial_T \\ 0 & \omega_0^{-2}\partial_t\partial_T \end{pmatrix}. \tag{52}$$

We now seek solutions order by order.

$\mathcal{O}(\varepsilon^{1/2})$ At this order, the solution to the linear problem is given by (16), where k and ω satisfy dispersion relation (17). As k will be determined by the length scale of the Bragg grating structure, we prefer to solve (17) for ω as a function of k:

$$\omega^2 = \frac{1}{2}\left(n^2\omega_0^2 + k^2\right) \pm \frac{1}{2}\sqrt{(n^2\omega_0^2 + k^2)^2 - 4\omega_0^2k^2}. \tag{53}$$

Equation (53) has two roots corresponding to each choice of sign. In the limit as $\omega_0 \to \infty$, the root corresponding to the plus sign diverges to ∞, while the root corresponding to the minus sign approaches the finite value $n^2\omega^2 = k^2$, as noted in Section 3.1. We examine a pair of backward and forward propagating modes in Bragg resonance with the fiber and having slowly varying amplitudes,

$$\begin{pmatrix} E_0 \\ P_0 \end{pmatrix} = \left(E_+(Z,T)e^{i(k_Bz-\omega_Bt)} + E_-(Z,T)e^{-i(k_Bz+\omega_Bt)} + c.c.\right)\begin{pmatrix} 1 \\ \gamma_B \end{pmatrix}, \tag{54}$$

where

$$k_B = \frac{\pi}{d}, \tag{55}$$

$$\gamma_B = \frac{n^2-1}{1-(\frac{\omega_B}{\omega_0})^2}, \tag{56}$$

and ω_B is a root of (53) for the minus sign choice.

$\mathcal{O}(\varepsilon^{3/2})$ The equation at this order is

$$\mathcal{L}_0\begin{pmatrix} E_1 \\ P_1 \end{pmatrix} = -\mathcal{L}_1\begin{pmatrix} E_0 \\ P_0 \end{pmatrix} + \begin{pmatrix} 0 \\ 2\nu\cos(2k_Bz)P_0 + \phi P_0^3 \end{pmatrix}. \tag{57}$$

Substituting in the solution to the $\mathcal{O}(\varepsilon^{1/2})$ equation, we find

$$\begin{aligned} \mathcal{L}_0\begin{pmatrix} E_1 \\ P_1 \end{pmatrix} = {} & \begin{pmatrix} 2i\,(k_B\partial_Z E_+ + \omega_B(\gamma_B+1)\partial_T E_+) \\ \frac{2i\gamma_B\omega_B}{\omega_0^2}\partial_T E_+ + \gamma_B\nu E_- + 3\gamma_B^3\phi(|E_+|^2 + 2|E_-|^2)E_+ \end{pmatrix} e^{i(k_Bz-\omega_Bt)} \\ & + \begin{pmatrix} 2i\,(-k_B\partial_Z E_- + \omega_B(\gamma_B+1)\partial_T E_-) \\ \frac{2i\gamma_B\omega_B}{\omega_0^2}\partial_T E_- + \gamma_B\nu E_+ + 3\gamma_B^3\phi(|E_-|^2 + 2|E_+|^2)E_- \end{pmatrix} e^{-i(k_Bz+\omega_Bt)} \\ & + \begin{pmatrix} 0 \\ \gamma_B^3\phi E_+^3 \end{pmatrix} e^{3i(k_Bz-\omega_Bt)} \end{aligned}$$

$$
\begin{aligned}
&+\begin{pmatrix} 0 \\ 3\gamma_B^3\phi E_+^2 E_- \end{pmatrix} e^{i(k_B z-3\omega_B t)} \\
&+\begin{pmatrix} 0 \\ 3\gamma_B^3\phi E_+ E_-^2 \end{pmatrix} e^{-i(k_B z+3\omega_B t)} \\
&+\begin{pmatrix} 0 \\ \gamma_B^3\phi E_-^3 \end{pmatrix} e^{-3i(k_B z+\omega_B t)} \\
&+\begin{pmatrix} 0 \\ 3\gamma_B^3\phi E_+^2 E_-^* + \gamma_B \nu E_+ \end{pmatrix} e^{i(3k_B z-\omega_B t)} \\
&+\begin{pmatrix} 0 \\ 3\gamma_B^3\phi E_-^2 E_+^* + \gamma_B \nu E_- \end{pmatrix} e^{-i(3k_B z+\omega_B t)} + c.c. \qquad (58)
\end{aligned}
$$

Of the terms on the right-hand side of (58), only the first two are potentially resonant and may therefore give rise to secular growth in time, t. The nonresonance condition required to remove such resonances can be expressed as the requirement that the vector coefficients of $e^{i(k_B-\omega_B t)}$ and $e^{-i(k_B z+\omega_B t)}$ both lie in the column space of $\mathcal{L}_0(\omega_B, \pm k_B)$; see (51). Equivalently, we require that the inner product of each of these vectors with the vector $(-\mathcal{L}_{02,1}, \mathcal{L}_{01,1})$ be equal to zero. This yields the Nonlinear Coupled Mode Equations (NLCME):

$$i\left(\partial_T E_+ + v_g \partial_Z E_+\right) + \kappa E_- + \Gamma(|E_+|^2 + 2|E_-|^2)E_+ = 0, \qquad (59a)$$

$$i\left(\partial_T E_- - v_g \partial_Z E_-\right) + \kappa E_+ + \Gamma(|E_-|^2 + 2|E_+|^2)E_- = 0. \qquad (59b)$$

Here

$$v_g = \omega'(k_B) = k'(\omega_B)^{-1} = \frac{k_B(\frac{\omega_B^2}{\omega_0^2} - 1)}{\omega_B\left(\frac{\omega_B^2}{\omega_0^2} - (1+\gamma_B)\right)} \qquad (60)$$

is the group velocity, and the coupling and nonlinearity parameters are

$$\kappa = \frac{\omega_B(n^2-1)}{2\left(n^2 - 1 + \left(1 - \frac{\omega_B^2}{\omega_0^2}\right)^2\right)}\nu, \qquad \Gamma = \frac{3\gamma_B^3\omega_B^2}{k_B(1-\frac{\omega_B^2}{\omega_0^2})}\phi. \qquad (61)$$

Our proof of validity of NLCME on timescales of order ε^{-1} requires that we solve explicitly for E and P through order ε. We solve (58) and obtain

$$\begin{pmatrix} E_1 \\ P_1 \end{pmatrix} = \sum_{\substack{a=\pm1,\pm3 \\ b=1,3}} \begin{pmatrix} E_1^{(a,b)} \\ P_1^{(a,b)} \end{pmatrix} + c.c., \qquad (62)$$

such that for $(a, b) \neq (\pm 1, 1)$,

$$\mathcal{L}_0 \begin{pmatrix} E_1^{(a,b)} \\ P_1^{(a,b)} \end{pmatrix} = \begin{pmatrix} 0 \\ S^{(a,b)} \end{pmatrix} e^{i(ak_B z - b\omega_B t)}, \qquad (63)$$

where $S^{(a,b)}$ is determined in equation (58), and for $(a, b) = (\pm 1, 1)$, the right-hand side is determined by using (59) to eliminate $\partial_T E_\pm$ from the first two terms of (58). Once

this is done, these terms take the form of the nonnull eigenvectors of $\mathcal{L}_0$ and solving this part of the equation becomes a trivial linear algebra problem. In this way we may represent the approximate solution using only $E_\pm$ and their Z-derivatives, so that L^2 and H^s estimates on solutions to the NLCME suffice for proof of the main theorem.

5. The Initial Value Problem for AMLE and NLCME

Our proof of the validity of NLCME as an approximation to AMLE requires some a priori knowledge of the solutions of these equations. In this section we outline the theory of the initial value problems for AMLE and NLCME and collect the necessary facts for the proof of the main theorem.

Both AMLE and NLCME are semilinear hyperbolic systems whose initial value problems can be expressed in the form

$$\begin{aligned} \partial_t \Phi(t) &= -iA\Phi(t) + J[\Phi(t)], \\ \Phi(t=0) &= \Phi_0. \end{aligned} \tag{64}$$

Here, A is a self-adjoint operator on a Hilbert space $\mathcal{H}$ and J is a nonlinear mapping from $\mathcal{H}$ to itself and $\Phi_0 \in \mathcal{H}$.

We first indicate how AMLE and NLCME can be expressed in this form and then show how the general theory and *energy estimates* can be used to conclude the existence of global in time solutions.

AMLE:

To write the AMLE system, (6), as a first-order system we use the variables E, B, P and $Q \equiv \partial_t P$. The AMLE system then becomes

$$\begin{aligned} \partial_t E &= \partial_z B - Q, \\ \partial_t B &= \partial_z E, \\ \partial_t P &= Q, \\ \partial_t Q &= -\omega_0^2(1 - 2\varepsilon\nu\cos(2k_B z))P - \omega_0^2 g(P, z) + \omega_0^2(n^2 - 1)E. \end{aligned} \tag{65}$$

We now write (65) in a more compact form. Let

$$\vec{u} = \begin{pmatrix} E \\ B \\ P \\ Q \end{pmatrix} \qquad \text{and} \qquad \mathcal{M} = \begin{pmatrix} 0 & \partial_z & 0 & -1 \\ \partial_z & 0 & 0 & 0 \\ 0 & 0 & 0 & 1 \\ \omega_0^2(n^2-1) & 0 & -\omega_0^2 & 0 \end{pmatrix}. \tag{66}$$

Then, the full system may be written

$$\partial_t \vec{u} = \mathcal{M}\vec{u} + \omega_0^2 \hat{e}_4 \left(2\varepsilon\nu\cos(2k_B z)P - g(P, z)\right), \tag{67}$$

where $\hat{e}_4 = (0, 0, 0, 1)^T$. Thus,

$$\Phi = \vec{u}, \; A = i\mathcal{M}, \tag{68}$$

$$J[\Phi] = \omega_0^2 \hat{e}_4 \left(2\varepsilon\nu\cos(2k_B z)P - g(P, z)\right). \tag{69}$$

NLCME:

NLCME can be written in the form (64) with the definitions

$$\Phi = \begin{pmatrix} E_+ \\ E_- \end{pmatrix}, \tag{70}$$

$$\sigma^1 = \begin{pmatrix} 0 & 1 \\ 1 & 0 \end{pmatrix}, \tag{71}$$

$$A = -iv_g\partial_Z - \kappa\sigma^1, \tag{72}$$

$$J[\Phi] = i\Gamma \begin{pmatrix} \left(|E_+|^2 + 2|E_-|^2\right) E_+ \\ \left(|E_-|^2 + 2|E_+|^2\right) E_- \end{pmatrix}. \tag{73}$$

We now formulate the general initial value problem (64) as an equivalent integral equation,

$$\Phi(t) = e^{-iAt}\Phi_0 + \int_0^t e^{-iA(t-s)} J[\Phi(s)]\, ds. \tag{74}$$

It is elementary to show [38] using the contraction mapping principle that in both examples, for any initial condition Φ_0 in the Hilbert space $\mathcal{H} = H^1$, there is a maximal time $T_{max} = T_{max}(\|\Phi_0\|_{H^1}) > 0$ and a solution $\Phi(t)$ of (74), which is defined for $t \in [0, T_{max})$, the maximal time interval of existence. The solution $\Phi(t) \in H^1$ for each $t \in [0, T_{max})$ and the function $t \mapsto \|\Phi(t)\|_{H^1}$ is continuous for $t \in [0, T_{max})$. Finally, either $T_{max} < \infty$ or $T_{max} = \infty$. If $T_{max} < \infty$, then

$$\lim_{t \nearrow T_{max}} \|\Phi(t)\|_{H^1} = \infty, \tag{75}$$

and we say that the solution $\Phi(t)$ blows up at time T_{max} in H^1. As we have seen in Theorem 2 of Section 3, in the absence of material dispersion, solutions of the AMLE system do develop singularities in their gradients in finite time. We claim that for both dispersive systems AMLE and NLCME no singularities form:

Theorem 3. *For initial data in H^1, $T_{max} = \infty$. That is, AMLE (under Hypothesis 1 below on the nonlinearity) and NLCME have H^1 solutions that are global in time.*

To prove this theorem, it suffices to show that if T_1 is an arbitrary time, then the H^1 norm of any of the components of $\Phi(t)$ satisfies an estimate

$$\|\Phi_j(t)\|_{H^1} \le C(T_1). \tag{76}$$

The constant $C(T_1)$ may depend on and even grow with T_1, but must be finite for finite values of T_1. To prove (76), we use a combination of the conservation laws associated with AMLE and NLCME as well as direct a priori estimates on the evolution equations. We consider the cases of AMLE and NLCME individually.

Proof of Theorem 3 for AMLE. We use the formulation for AMLE given in (67) or, equivalently, (65). Our proof makes use of the following technical assumption on the nonlinear term that ensures the existence of global solutions for arbitrary size H^1 data:

Hypothesis 1. *There exists a constant C, such that for all z,*

$$|g(P,z)| + |\partial_z g(P,z)| \le C|P|, \qquad |\partial_P g(P,z)| \le C. \tag{77}$$

The first step is to derive an *energy estimate* for AMLE. Taking the dot product of (67) with the vector $(E,\, B,\, (n^2-1)^{-1}P,\, \omega_0^{-2}(n^2-1)^{-1}Q)$ yields

$$\begin{aligned}
&\frac{d}{dt}\frac{1}{2}\int\left(E^2 + B^2 + \frac{1}{n^2-1}P^2 + \frac{1}{\omega_0^2(n^2-1)}Q^2\right)dz \\
&\quad = \frac{2\varepsilon\nu}{n^2-1}\int \cos(2k_B z)\,P\,Q\,dz - \frac{1}{n^2-1}\int g(P,z)\,Q\,dz \\
&\quad \le C\int (P^2+Q^2)\,dz.
\end{aligned} \tag{78}$$

The previous inequality follows from Hypothesis 1. It follows that

$$\|\vec{u}(t)\|_{L^2}^2 \le \|\vec{u}_0\|_{L^2}^2 + C_1\int_0^t \|\vec{u}(s)\|_{L^2}^2\,ds \tag{79}$$

for some positive constant C_1 and therefore, by Gronwall's inequality,

$$\|\vec{u}(t)\|_{L^2} \le \|\vec{u}_0\|_{L^2}\, e^{C_1 t}. \tag{80}$$

Estimates for the L^2 norm of $\partial_z\vec{u}$ are obtained in a similar manner. We first differentiate equation (67) for $\vec{u}$ with respect to z, and then take the dot product with $(\partial_z E,\, \partial_z B,\, (n^2-1)^{-1}\partial_z P,\, \omega_0^{-2}(n^2-1)^{-1}\partial_z Q)$ and obtain

$$\begin{aligned}
&\frac{d}{dt}\frac{1}{2}\int\left(E_z^2 + B_z^2 + \frac{1}{n^2-1}P_z^2 + \frac{1}{\omega_0^2(n^2-1)}Q_z^2\right)dz \\
&\quad = \frac{\varepsilon\nu}{n^2-1}\int[2\cos(2k_B z)\,P_z Q_z - 4k_B\sin(2k_B z)\,P\,Q_z]\,dz \\
&\qquad - \frac{1}{n^2-1}\int \partial_P g(P,z)\,P_z Q_z\,dz - \frac{1}{n^2-1}\int \partial_z g(P,z)\,Q_z\,dz \\
&\quad \le C\int\left(P^2+Q^2+P_z^2+Q_z^2\right)dz.
\end{aligned} \tag{81}$$

This, together with the above L^2 energy estimate, can be used to conclude, by Gronwall's inequality,

$$\|\vec{u}\|_{H^1} \le \|\vec{u}_0\|_{H^1}\, e^{C_2 t}. \tag{82}$$

Since the H^1 norm of $\vec{u}$ grows at worst exponentially, we conclude that $T_{max} = \infty$. This completes the proof of H^1 existence for solutions to AMLE. □

Proof of Theorem 3 for NLCME

Proposition 1. *Let $\vec{E} = (E_+, E_-)$ satisfy system (59) with initial conditions $\vec{E}(0) \in H^s$ for $s \ge 1$.*[9] *Then there exists $C_s = C_s(\|\vec{E}(0)\|_{H^s}, T)$ such that $\|\vec{E}(T)\|_{H^s} \le C_s(\|\vec{E}(0)\|_{H^s}, T)$. Moreover, $C(x_1, x_2) \to 0$ as $x_1 \to 0$.*

[9] In our proof of Theorem 1, we use this result for $s \le 3$.

Proof. It is easy to see that system (59) preserves the L^2 norm. To obtain this and higher L^p bounds on $E_\pm$, we multiply both sides of (59a) by $|E_+|^{2\sigma}E_+^*$ and (59b) by $|E_-|^{2\sigma}E_-^*$, add them, and take the imaginary part, yielding

$$\frac{1}{\sigma+1}\left(\partial_T(|E_-|^{2\sigma+2}+|E_+|^{2\sigma+2})\right)+v\partial_Z(|E_+|^{2\sigma+2}-|E_-|^{2\sigma+2}) \\ +i\Gamma(E_+E_-^*+E_-E_+^*)(|E_+|^{2\sigma}-|E_-|^{2\sigma})=0. \tag{83}$$

If $\sigma=0$, then the last term is identically zero, showing that $\|\vec{E}\|_2^2$ is conserved.[10] If $\sigma>0$, then we may bound $\|\vec{E}\|$ using Gronwall's inequality,

$$\begin{aligned}\frac{d}{dT}\|\vec{\mathcal{E}}\|_{2\sigma+2}^{2\sigma+2} &\le c(\sigma+1)\|\vec{\mathcal{E}}\|_{2\sigma+2}^{2\sigma+2},\\ \|\vec{\mathcal{E}}\|_{2\sigma+2}^{2\sigma+2} &\le \|\vec{\mathcal{E}}_0\|_{2\sigma+2}e^{c(\sigma+1)T},\\ \|\vec{\mathcal{E}}\|_{2\sigma+2} &\le \|\vec{\mathcal{E}}_0\|_{2\sigma+2}e^{cT/2}.\end{aligned} \tag{84}$$

Letting $p=2\sigma+2$, this is just

$$\|\vec{\mathcal{E}}\|_p \le \|\vec{\mathcal{E}}_0\|_p e^{cT/2}. \tag{85}$$

As c is independent of p, this estimate holds for L^∞.

The L^∞ bound can then be used to bound growth rates of the L^p norms of $\partial_Z E_\pm$ in terms of T. Taking Z-derivatives of the NLCME and performing a similar calculation with $\sigma=0$ yields

$$\begin{aligned}\frac{d}{dT}\|\partial_Z\vec{\mathcal{E}}\|_2^2 &\le c\|\vec{\mathcal{E}}\cdot\partial_Z\vec{\mathcal{E}}\|_2^2\\ &\le c\|\vec{\mathcal{E}}\|_{L^\infty}^2\|\partial_Z\vec{\mathcal{E}}\|_{L^2}^2\\ &\le c\|\vec{\mathcal{E}}_0\|_{L^\infty}^2e^{2cT}\|\partial_Z\vec{\mathcal{E}}\|_{L^2}^2,\end{aligned} \tag{86}$$

so that

$$\|\vec{\mathcal{E}}\|_{H^1} \le \|\vec{\mathcal{E}}_0\|_{H^1}e^{c(e^{cT}-1)}. \tag{87}$$

This shows that we can indeed bound the solutions of NLCME in H^1 and control them for times $T=\mathcal{O}(1)$, i.e., $t=\mathcal{O}(\frac{1}{\varepsilon})$. Proceeding similarly, we can derive bounds in higher Sobolev spaces, specifically H^2 norms like $e^{ce^{ce^{cT}}}$, and H^3 bounds like $e^{ce^{ce^{ce^{cT}}}}$, thus completing the proof of Proposition 1, and hence, by the comments preceding Theorem 3, of that theorem. □

6. Validity of NLCME for Times, t, of $\mathcal{O}(\varepsilon^{-1})$; Proof of Theorem 1

We shall work with the formulation of AMLE given in (65).

We proceed under the following hypothesis concerning the nonlinearity $g(P,z)$ and its derivative $\partial_P g(P,z)$ for small P:

[10] Recall that $\|\vec{\mathcal{E}}\|_p^p=\int(|E_+|^p+|E_-|^p)\,dZ$.

Hypothesis 2. *Assume g has partial derivative of order ≤ 4 with respect to P and has one partial derivative with respect to z that is continuous. Assume further that $g(0,z) = (\partial_P g)(0,z) = (\partial_P^2 g)(0,z) = 0$, and $\phi \equiv -\frac{1}{3!}(\partial_P^3 g)(0,z) \neq 0$ and is independent of z, and make the analogous assumptions for $\partial_z g$. Therefore, there exists a positive constant, C, such that for all z and all P_1, P_2 with $|P_1| + |P_2|$ sufficiently small,*

$$\begin{aligned} |g(P_1+P_2,z) - g(P_1,z)| &\leq C\left(|P_1|^2 + |P_2|^2\right)|P_2|, \\ |\partial_P g(P_1+P_2,z) - \partial_P g(P_1,z)| &\leq C\left(|P_1| + |P_2|\right)|P_2|, \\ |\partial_z g(P_1+P_2,z) - \partial_z g(P_1,z)| &\leq C\left(|P_1|^2 + |P_2|^2\right)|P_2|. \end{aligned} \tag{88}$$

To obtain an approximate solution of (65), we require, in addition to our approximations of E and P, approximations to B and Q through first order in ε. We use the relation $\partial_t B(t,z) = \partial_z E(t,z)$ to obtain the relations

$$\partial_t B_0 = \partial_z E_0, \tag{89}$$

$$\partial_t B_1 = -\partial_T B_0 + \partial_z E_1 + \partial_Z E_0. \tag{90}$$

Also, using $Q = \partial_t P$, we find

$$Q_0 = \partial_t P_0, \tag{91}$$

$$Q_1 = \partial_t P_1 + \partial_T P_0. \tag{92}$$

We may then define

$$X^{\varepsilon}_{app} = \varepsilon^{\frac{1}{2}}\left(X_0 + \varepsilon X_1\right) \quad \text{for } X = E,\, B,\, P, \text{ or } Q, \tag{93}$$

and write our approximate solution to (65) as

$$\vec{u}^{\varepsilon}_{app} = \begin{pmatrix} E^{\varepsilon}_{app} \\ B^{\varepsilon}_{app} \\ P^{\varepsilon}_{app} \\ Q^{\varepsilon}_{app} \end{pmatrix}. \tag{94}$$

The full solution to AMLE may therefore be written as

$$\vec{u} \equiv \vec{u}^{\varepsilon}_{app}(t,z;T,Z) + \varepsilon \vec{R}^{\varepsilon}(t,z), \tag{95}$$

where

$$\vec{R}^{\varepsilon} = \begin{pmatrix} R^{\varepsilon}_E \\ R^{\varepsilon}_B \\ R^{\varepsilon}_P \\ R^{\varepsilon}_Q \end{pmatrix} \tag{96}$$

denotes the error term. To prove the main theorem, it suffices to prove that for any $T_0 > 0$, $\vec{R}^{\varepsilon}$ remains bounded of order one, in an appropriate norm, uniformly for ε sufficiently small and $0 \leq t \leq T_0/\varepsilon$.

We now derive the equation for $\vec{R}^{\varepsilon}$. Viewing t, z, T, Z as independent variables, (67), the equation for $\vec{u}^{\varepsilon}$ can be rewritten as

$$\partial_t \vec{u} = \mathcal{M}\vec{u} - \varepsilon \mathcal{N}\vec{u} + \omega_0^2 \hat{e}_4\left(2\varepsilon\nu\cos(2k_B z)P - g(P,z)\right), \tag{97}$$

where

$$\mathcal{N} = \begin{pmatrix} \partial_T & -\partial_Z & 0 & 0 \\ -\partial_Z & \partial_T & 0 & 0 \\ 0 & 0 & \partial_T & 0 \\ 0 & 0 & 0 & \partial_T \end{pmatrix}. \tag{98}$$

To obtain an evolution equation for $\vec{R}^\varepsilon$, we substitute (95) into (97) to obtain

$$\begin{aligned} \partial_t(\vec{u}^\varepsilon_{app} + \varepsilon\vec{R}^\varepsilon) \;=\; & \mathcal{M}(\vec{u}^\varepsilon_{app} + \varepsilon\vec{R}^\varepsilon) + \varepsilon\mathcal{N}(\vec{u}^\varepsilon_{app} + \varepsilon\vec{R}^\varepsilon) \\ & + \omega_0^2\hat{e}_4(2\varepsilon\nu\cos(2k_Bz)(P^\varepsilon_{app} + \varepsilon R^\varepsilon_P) - g(P^\varepsilon_{app} + \varepsilon R^\varepsilon_P, z)). \end{aligned} \tag{99}$$

We may then eliminate from this two equations obtained during the multiple scales expansion,

$$(\partial_t - \mathcal{M})\,\vec{u}_0 \;=\; 0; \tag{100a}$$

$$(\partial_t - \mathcal{M})\,\vec{u}_1 \;=\; -\mathcal{N}\vec{u}_0 + 2\omega_0^2\hat{e}_4\cos(2k_Bz)P_0 + \omega_0^2\hat{e}_4\phi P_0^3, \tag{100b}$$

to leave an equation for the evolution of the error alone

$$\begin{aligned} (\partial_t - \mathcal{M})\vec{R}^\varepsilon \;=\; & -\varepsilon^{\frac{3}{2}}\mathcal{N}\vec{u}_1 + 2\nu\hat{e}_4\cos(2k_Bz)(\varepsilon^{\frac{3}{2}}P_1 + \varepsilon R^\varepsilon_P) \\ & + \omega_0^2\hat{e}_4\left(-\varepsilon^{-1}g(P^\varepsilon_{app} + \varepsilon R^\varepsilon_P, z) + \varepsilon^{\frac{1}{2}}\phi P_0^3\right). \end{aligned} \tag{101}$$

To this, we add and subtract $\varepsilon^{-1}\omega_0^2\hat{e}_4 g(P^\varepsilon_{app}, z)$ to obtain

$$\begin{aligned} (\partial_t - \mathcal{M})\vec{R}^\varepsilon \;=\; & -\varepsilon^{\frac{3}{2}}\mathcal{N}\vec{u}_1 + 2\nu\hat{e}_4\cos(2k_Bz)(\varepsilon^{\frac{3}{2}}P_1 + \varepsilon R^\varepsilon_P) \\ & + \varepsilon^{-1}\omega_0^2\hat{e}_4\left(g(P^\varepsilon_{app}, z) - g(P^\varepsilon_{app} + \varepsilon R^\varepsilon_P, z)\right) \\ & + \omega_0^2\hat{e}_4\left(-\varepsilon^{-1}g(P^\varepsilon_{app}, z) + \varepsilon^{\frac{1}{2}}\phi P_0^3\right) \\ =\; & 2\varepsilon\nu\hat{e}_4\cos(2k_Bz)R^\varepsilon_P \\ & + \varepsilon^{-1}\omega_0^2\hat{e}_4\left(g(P^\varepsilon_{app}, z) - g(P^\varepsilon_{app} + \varepsilon R^\varepsilon_P, z)\right) + \varepsilon^{-1}\vec{\rho}, \end{aligned} \tag{102}$$

where

$$\vec{\rho} = -\varepsilon^{\frac{5}{2}}\mathcal{N}\vec{u}_1 + \varepsilon^{\frac{5}{2}}\omega_0^2 2\nu\cos(2k_Bz)P_1 + \omega_0^2\left(\varepsilon^{\frac{3}{2}}\phi P_0^3 - g(P^\varepsilon_{app}, z)\right) \tag{103}$$

is the *residual*, essentially the amount by which u^ε_{app} fails to solve (67).

We now consider the formal size of the second and third terms on the right-hand side of (102). Since $P^\varepsilon_{app} + \varepsilon R^\varepsilon_P = \varepsilon^{\frac{1}{2}}(P_0 + \varepsilon P_1 + \varepsilon^{\frac{1}{2}}R^\varepsilon_P)$ and $g(P, z) \sim \phi P^3$, the second term of (102) is $\mathcal{O}(\varepsilon)$. We further note that since $\vec{u}^\varepsilon_{app}$ is an approximate solution through order ε, the residual $\vec{\rho}$ is formally of order ε^2 and so the third term of (102) is $\mathcal{O}(\varepsilon)$. In order to control this final term, we must calculate the approximate solution including terms formally of order $\varepsilon^{\frac{3}{2}}$ and also require that $E_\pm$ be in the Sobolev space H^3.

From this discussion, we expect that, for times of order ε^{-1}, $\vec{R}^\varepsilon$ will be bounded. For convenience, we introduce a notation that makes explicit the expected size of the residual:

$$\varepsilon\vec{r} = \varepsilon^{-1}\vec{\rho}. \tag{104}$$

It is then clear that in order to bound $\vec{R}^\varepsilon$ we will first need to bound $\vec{r}$.

Proposition 2 (Estimation of the residual). *Let (E_+, E_-) be a solution of the NLCME system (59). Then there exists a constant $c > 0$ depending on k and the Sobolev norms of $E_\pm$ of order up to three, but independent of ε such that for all $0 \le t \le T_0\varepsilon^{-1}$,*

$$\|\vec{r}\|_{L^\infty} \le c\,\varepsilon^{1/2}; \tag{105}$$

$$\|\vec{r}\|_{H^1} \le c. \tag{106}$$

This proposition is a simple consequence of the explicit expression for $\vec{r}$ (defined in terms of $\vec{\rho}$) given in (103), and of Proposition 1.

Proposition 3. *Let (E_+, E_-) be a solution of the NLCME system (59). Then there exist $\varepsilon_0 > 0$ and $C_0 > 0$ s.t. if $0 \le \varepsilon \le \varepsilon_0$, the solution of (102) satisfies $\|\vec{R}^\varepsilon\|_{H^1} \le C_0$ for all $0 \le t \le T_0\varepsilon^{-1}$.*

These propositions imply Theorem 1.

6.1. Proof of Proposition 3: Estimates on the Error $\vec{R}^\varepsilon$

Recall that the evolution equation for $\vec{R}^\varepsilon$ is given by

$$\partial_t \vec{R}^\varepsilon = \mathcal{M}\vec{R}^\varepsilon + \hat{e}_4\omega_0^2\left(2\varepsilon\nu\cos(2k_Bz)R_P^\varepsilon - \frac{1}{\varepsilon}\left(g(P,z) - g(P_{app}^\varepsilon, z)\right)\right) + \varepsilon\vec{r}. \tag{107}$$

Motivated by the energy estimates used in Section 5, we introduce the weighted norms

$$|||\vec{R}^\varepsilon|||^2 \equiv \int \vec{R}^\varepsilon \cdot \Lambda\vec{R}^\varepsilon\,dz$$

$$= \int_{-\infty}^{\infty}\left(R_E^{\varepsilon\,2} + R_B^{\varepsilon\,2} + \frac{R_P^{\varepsilon\,2}}{n^2-1} + \frac{R_Q^{\varepsilon\,2}}{\omega_0^2(n^2-1)}\right)dz, \tag{108}$$

$$|||\vec{R}^\varepsilon|||_{H^1}^2 \equiv |||\vec{R}^\varepsilon|||^2 + |||\partial_z\vec{R}^\varepsilon|||^2, \tag{109}$$

where the weight Λ is given by the matrix

$$\Lambda = \mathrm{diag}\left(1, 1, \frac{1}{n^2-1}, \frac{1}{\omega_0^2(n^2-1)}\right).$$

These norms are clearly equivalent to the standard L^2 and H^1 norms.

Then we have

$$\frac{d}{dt}\frac{1}{2}|||\vec{R}^\varepsilon|||^2 = \frac{1}{n^2-1}\int\left(2\varepsilon\nu\cos(2k_Bz)R_P^\varepsilon + \frac{1}{\varepsilon}[g(P_{app}^\varepsilon, z) - g(P_{app}^\varepsilon + \varepsilon R_P^\varepsilon, z)]\right)R_Q^\varepsilon dz$$

$$+ \varepsilon\int \vec{R}^\varepsilon \cdot \Lambda\vec{r}\,dz. \tag{110}$$

Similarly, differentiation of (107) with respect to z and left multiplication by $(\partial_z \vec{R}^\varepsilon)^{\mathrm{T}}\Lambda$ yields

$$\begin{aligned}\frac{d}{dt}\frac{1}{2}|||\partial_z \vec{R}^\varepsilon|||^2 \;=\; & \frac{\varepsilon\nu}{n^2-1}\int \left(2\cos(2k_B z)\partial_z R_P^\varepsilon \partial_z R_Q^\varepsilon - 4k_B \sin(2k_B z) R_P^\varepsilon \partial_z R_Q^\varepsilon\right) dz \\ & + \frac{1}{\varepsilon}\int \left(\partial_P g(P_{app}^\varepsilon, z) - \partial_P g(P_{app}^\varepsilon + \varepsilon R_P^\varepsilon, z)\right) \partial_z P_{app}^\varepsilon \partial_z R_Q^\varepsilon \, dz \\ & - \int \partial_P g(P_{app} + \varepsilon R_P^\varepsilon, z)\partial_z R_P^\varepsilon R_Q^\varepsilon \, dz \\ & + \frac{1}{\varepsilon}\int \left(\partial_z g(P_{app}^\varepsilon, z) - \partial_z g(P_{app}^\varepsilon + \varepsilon R_P^\varepsilon, z)\right) \partial_z R_Q^\varepsilon \, dz \\ & + \varepsilon \int \partial_z \vec{R}^\varepsilon \cdot \Lambda \partial_z \vec{r} \, dz. \end{aligned} \tag{111}$$

Application of Hypothesis 2, the L^∞ bound on solutions of NLCME of Proposition 2, Sobolev's inequality[11] [22], and interpolation yields

$$\frac{d}{dt}|||\vec{R}^\varepsilon|||^2 \le C_1\varepsilon|||\vec{R}^\varepsilon|||^2 + C_2\varepsilon^2|||\vec{R}^\varepsilon|||_{H^1}^4 + \varepsilon\|\vec{r}\|_{L^2}|||\vec{R}^\varepsilon||| \tag{112}$$

and

$$\frac{d}{dt}|||\partial_z \vec{R}^\varepsilon|||^2 \le C_1\varepsilon|||\vec{R}^\varepsilon|||_{H^1}^2 + C_2\varepsilon^2|||\vec{R}^\varepsilon|||_{H^1}^4 + C_3\varepsilon\|\partial_z\vec{r}\|_{L^2}\,|||\vec{R}^\varepsilon|||_{H^1}. \tag{113}$$

Estimates (112) and (113) imply

$$\frac{d}{dt}|||\vec{R}^\varepsilon|||_{H^1}^2 \le C\,\left(\varepsilon|||\vec{R}^\varepsilon|||_{H^1}^2 + \varepsilon^2|||\vec{R}^\varepsilon|||_{H^1}^4 + \varepsilon\|\vec{r}\|_{H^1}\,|||\vec{R}^\varepsilon|||_{H^1}\right). \tag{114}$$

If $\vec{R}^\varepsilon(0) = 0$, then by equation (107), $\|\vec{R}^\varepsilon\| \neq 0$ for $t > 0$. We therefore assume $\|\vec{R}^\varepsilon(0)\| > 0$. We may then let $\zeta(t) = |||\vec{R}^\varepsilon|||(t)$. Then (76) and the H^1 bound on $\vec{r}$ from Proposition 2 implies

$$\frac{d\zeta}{dt} \le C\varepsilon\left(1 + \zeta + \varepsilon\zeta^3\right). \tag{115}$$

This differential inequality is easily solved, and we conclude that, for any $T_0 > 0$,

$$\|\vec{R}^\varepsilon(t)\|_{H^1} \le C\,|||\vec{R}^\varepsilon(t)||| \le C(T_0) \quad \text{for } 0 \le t \le T_0\varepsilon^{-1}. \tag{116}$$

Finally, we note that, as

$$\vec{u} = \vec{u}_{NLCME} + \varepsilon^{\frac{3}{2}}\vec{u}_1 + \varepsilon\vec{R}^\varepsilon, \tag{117}$$

then

$$\|\vec{u} - \vec{u}_{NLCME}\|_{H^1} \le \varepsilon^{\frac{3}{2}}\|\vec{u}_1\|_{H^1} + \varepsilon\|\vec{R}^\varepsilon\|_{H^1}. \tag{118}$$

[11] $\|f\|_{L^\infty}^2 \le C\|f\|_{L^2}\|\partial_z f\|_{L^2}$.

The estimates on $E_\pm$ guarantee that the first term on the right-hand side is $\mathcal{O}(\varepsilon)$, and Proposition 3 guarantees that the second term is $\mathcal{O}(\varepsilon)$. Thus,

$$\|\vec{u} - \vec{u}_{NLCME}\|_{H^1} \leq C\varepsilon \text{ for } 0 \leq t \leq T_0\varepsilon^{-1}. \tag{119}$$

This completes the proof. □

7. Numerical Demonstration—Gap Soliton Propagation and Decay

We initialize a wavepacket for AMLE with many oscillations and an envelope whose form is constructed using the gap soliton solution to the NLCME. The gap soliton decays exponentially away from its "center." We perform the simulations with periodic geometry. The period is chosen to be several gap soliton widths so that the solution is well localized away from the artificial period ends. The gap soliton initial condition is initialized within the central region of the domain, so that the localized structure is essentially unaffected by the boundary and propagates as though it were on an infinite spatial domain. In addition, we compute the evolution of a solution to the NLCME with corresponding envelope initial conditions, and use the formulae (54), (89), and (91) to construct approximate solutions to AMLE for comparison.

7.1. Numerical Methods

We use a "method of lines" approach, meaning that we first discretize in the spatial dimension, yielding a set of ordinary differential equations in t for the values of the solution at the discretization points. We compute solutions to AMLE as the first-order system given in (65). We restrict our computational domain to a finite period interval and discretize with about 16 points per wavelength. Derivatives are computed spectrally using discrete Fourier transforms [20]. That is, suppose $\mathcal{F}$ is the discrete Fourier transform, ξ is the dual variable to z, and $\vec{f}$ is a vector of discrete values of f. Then the approximate derivative is given by

$$\partial_z f = \left(\mathcal{F}^{-1} i\xi \mathcal{F}\right) \vec{f}.$$

The spatial discretization of system (65) may now be treated numerically as a system of ODEs. A fixed-step fourth-order explicit Runge-Kutta method is used to integrate the resulting system in time. Recall that an n-stage explicit Runge-Kutta method for a general evolution equation

$$\dot{y}(t) = f(y, t)$$

is given by [21]:

$$\begin{aligned} k_1 &= f(y_k, t_k), \\ k_i &= f\left(y_k + a_i \Delta t, t_k + \Delta t \sum_{j=1}^{i-1} b_{i,j} k_j\right), \qquad \text{for } i = 2, n, \\ y_{k+1} &= y_k + \sum_{i=1}^{n} c_i k_i. \end{aligned}$$

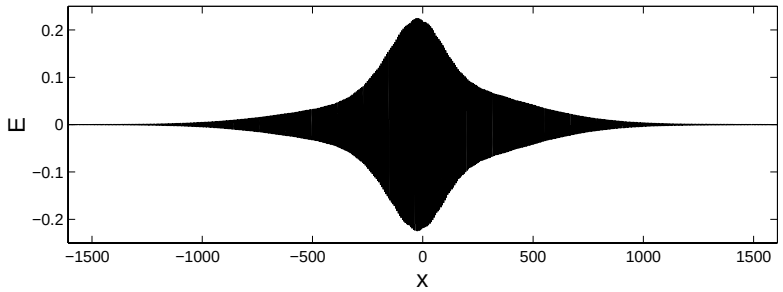

Fig. 7. The initial data for the electric field satisfying the SVEA.

Explicit methods tend to impose stability restrictions on the allowable step size for the time integration. However, in the case of the AMLE (65), this is simply that $\Delta t < C\Delta z$, which is a very mild restriction compared, for example, to the heat equation, for which $\Delta t < C\Delta z^2$. For most of our simulations, we work with about 16 points per wavelength, which gives $\Delta z \approx \frac{1}{3}$ and a comparable value for Δt.

Empirical convergence tests show the method to have fourth-order convergence in time, and constants of motion are also computed numerically and are shown to be conserved to 8 or 10 digits. A similar method is used for NLCME, though the accuracy is far less crucial as the solutions contain far fewer oscillations and vary on a slower timescale.

7.2. Numerical Verification

To numerically verify and explore the limits of Theorem 1, we solve both AMLE and NLCME under the SVEA scaling and compare $\vec{u}$ with $\sqrt{\varepsilon}\vec{u}_0$ by monitoring the quantity,

$$\text{Error}_\varepsilon(t) = \vec{u}^\varepsilon - \sqrt{\varepsilon}\vec{u}_0. \tag{120}$$

We do this for two values of ε, and check that the agreement scales appropriately as ε is decreased. This is done for $\varepsilon_1 = \frac{1}{32}$ and $\varepsilon_2 = \frac{1}{64}$, and so the error should be reduced by half between the two runs. For the purposes of verification, we take much larger values of the refractive index contrast ε than would be used in a physical experiment.

In Figure 7, we show a typical initial condition for the electric field E. The parameters used for this and all the numerical experiments described in this section are given in Appendix C. The envelope in this figure is 256 wavelengths long, and it is generated from a simulation with $\varepsilon = 1/64$. The shape of the electric field envelope as the wave propagates clearly illustrates the effect of the periodic medium on propagation. In Figure 8 we see that the electric field envelope (computed from "full" AMLE solutions) is "two humped" with the amplitude moving forward and backward between the humps at a faster rate than the envelope itself moves forward. In the same figure, we plot the location of the maximum of the electric field, and it becomes clear that the electric field maximum moves forward unsteadily, interrupted by a sequence of backward jumps. Also plotted

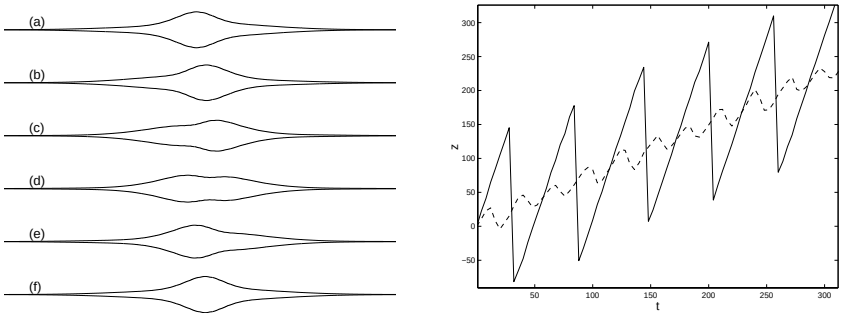

Fig. 8. (Left) The motion of the electric field by reflection and nonlinear regrouping. Between (a) and (c) the envelope moves forward, between (c) and (e) it is reflected backwards, and at (f) it has begun propagating forward again. (Right) The location of the maximum of E (solid line) and the location of the energy density maximum (dashed line) as a function of time, showing the effect of reflection off the grating (computed using the full AMLE system).

in this figure is the location of the energy density maximum,[12] which propagates more smoothly, since the contribution from the different fields is averaged.

Figure 9 shows the location of the electric field envelope at the beginning, middle, and end of the computed evolution period. This figure shows both the envelope computed from the AMLE and also the approximate envelope computed using the NLCME. To the "eyeball metric," the agreement appears to be quite close. More quantitatively, the success of this procedure is measured by an error-scaling factor given, for any norm,

$$\text{Error Scaling Factor} = \log_2 \frac{\|\text{Error}_\varepsilon\|(T_\varepsilon)}{\|\text{Error}_{\frac{\varepsilon}{2}}\|(T_{\frac{\varepsilon}{2}})}.$$

Then the numerics verify the asymptotic procedure if the scaling factor is equal to one. Figures 10 and 11 show that, computed in L^2, the error scales in agreement with Theorem 1, but that the L^∞ error is reduced by a factor of $2^{\frac{3}{2}}$. A general scaling argument shows this is reasonable. Consider a function $f(z)$ and let $f_\varepsilon(z) = \varepsilon^{\frac{3}{2}} f(\varepsilon z)$; then $\|f_\varepsilon\|_2 = \varepsilon \|f\|_2$, while $\|f_\varepsilon\|_\infty = \varepsilon^{\frac{3}{2}} \|f\|_\infty$. It appears that using H^1 estimates to control L^∞ estimates has cost us half a power of ε in our approximation of the error $\vec{R}^\varepsilon$.

7.3. Very Long Time Behavior

The error estimates of Theorem 1 tell us that the solution constructed from the NLCME and the full solution to AMLE should agree for times on the order of ε^{-1}. As a practical estimate, this may cause us some concern, as the width of the solitary wave is also $\mathcal{O}(\varepsilon^{-1})$ so that, on these timescales, the distance of propagation is the same order of magnitude as the width of the solution. It is therefore of interest to run our simulations for long times to see if the NLCME continues to provide a good approximation beyond what we have proven, or if the approximation breaks down completely.

[12] The energy density is the integrand on the left-hand side of equation (78).

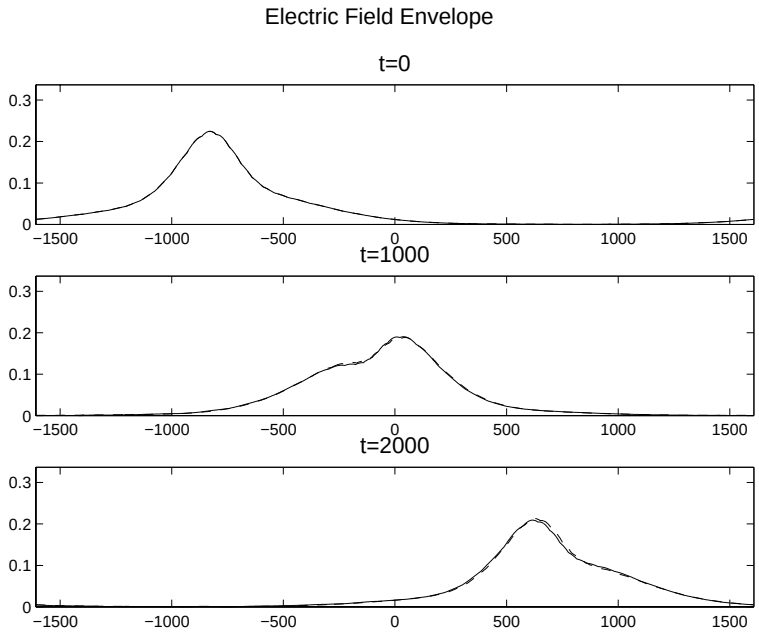

Fig. 9. The envelope of the electric field at the beginning, middle, and end of the computed evolution. Computations of both the AMLE envelope and its NLCME approximation are shown.

We run the simulation with $\varepsilon = 1/32$ and with $\omega_0 = 4$, allowing the evolution to continue to $t = 12000$, which is certainly larger than $\mathcal{O}(\varepsilon^{-1})$. By this time, the L^2 norm of the error is similar to the L^2 norm of the field itself and has stopped growing. Figure 12a shows that the envelopes of the full solution and the approximation no longer agree, but that they lie in approximately the same location. In Figure 12b, we see a blowup of the electric field and its approximation via the NLCME, which shows that the two solutions are completely out of phase with each other, so that pointwise estimates will not show any agreement between the solution and the approximation. Figure 12c, however, shows that the energy density of the full solution and the approximation continue to match very well. The solution has propagated about twenty times its own width (full width at half maximum or FWHM), and the centers of the two energy density plots are separated by about one-fifth of a FWHM. This is encouraging, as it suggests that, although the estimates of Theorem 1 no longer hold, the approximation and the full solution have basically remained together.

Although the description via the NLCME has broken down in the above discussion, the electric field has maintained the basic structure of a slowly modulated plane wave. Eventually, this very structure will break down and the solitary wave may itself break apart. This is shown in Figure 13 where a solitary wave, moving to the right, steepens at its trailing end and then begins to break up, while falling behind the AMLE envelope. In this figure, the parameters are as in Figure 12, except that $\omega_0 = 1$; this has the effect of decreasing the number of oscillations contained within the FWHM of the envelope from

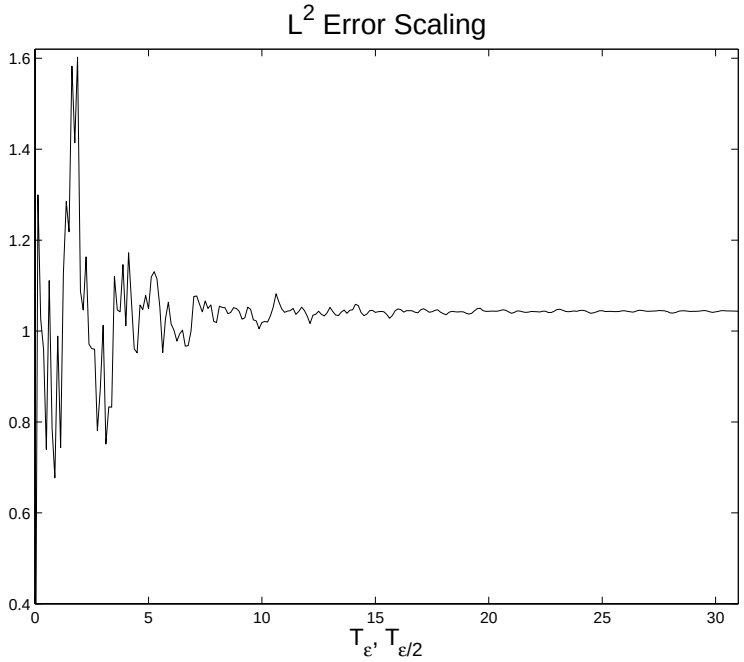

Fig. 10. Scaling of the error in L^2 as a function of the scaled time.

60 to 10, so that the separation of scales is much less pronounced. This much narrower envelope breaks up much faster than the solutions shown in previous plots. Although we have no precise measurement of this breakup time, it appears to happen on a timescale $t \sim \mathcal{O}(\varepsilon^{-2})$.

8. Summary and Discussion

In this paper we considered the propagation of high intensity light through a one-dimensional periodic structure. This was modeled by the anharmonic Maxwell Lorentz equations (AMLE), which incorporate the effects of material dispersion due to finite time response of the polarization field, photonic band dispersion due to the periodic structure, and nonlinearity (intensity effects). We first gave a detailed discussion of how these effects act individually and in various combinations, while also providing some numerical illustrations. We next considered AMLE solutions with spatially localized initial conditions, nearly monochromatic at the Bragg resonant carrier frequency and such that the effects of dispersion and nonlinearity are balanced. We proved that, over timescales of interest, the backward and forward propagating field envelopes satisfy nonlinear coupled mode equations (NLCME), which we derived from AMLE using multiple scale analysis. We also derived rigorous bounds on the deviation of the NLCME solutions from those of the original Maxwell-Lorentz model. Theorem 1, which describes this, is the main mathematical

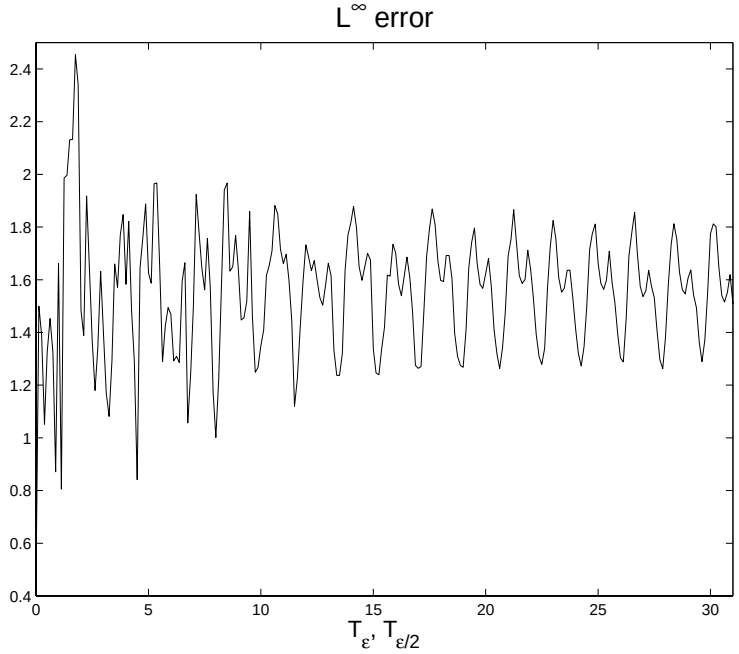

Fig. 11. Scaling of the error in L^∞ as a function of the scaled time.

result of the paper. We demonstrated its validity and probed its limitations via numerical simulation, as well as verifying that the ordering assumptions assumed in our analysis are consistent with the physical parameter magnitudes characteristic of experimental studies.

Two directions of great interest are the study of nonlinear phenomena in multidimensional photonic structures [3] and the extension of the present analysis to the case of more general inhomogeneous structures. The multiple scale techniques and the analysis used to obtain Theorem 1 can be applied to more general structures, e.g., periodic structures defined by a general Fourier series, index variations which are slow modulations of those considered, and "deep gratings." In the case of deep gratings, where the variation of the refractive index is not small, this requires the use of a multiscale expansion ansatz describing the slow modulation of Floquet-Bloch waves [10], rather than the plane waves we have used in the case of a system that is nearly translation-invariant in z.

A number of issues arose in our study which we presently discuss and raise as questions meriting further investigation:

(i) Numerical simulations suggest that NLCME continues to acceptably predict the location of the field energy on timescales for which the estimates used in proving Theorem 1 break down. Figure 12 shows that the coupled mode theory fails to predict the location of the individual peaks of the carrier wave while continuing to predict the location of the energy. It would be of interest to investigate whether there exists a weaker, more general framework, in which the AMLE solution is well described by the NLCME solution.

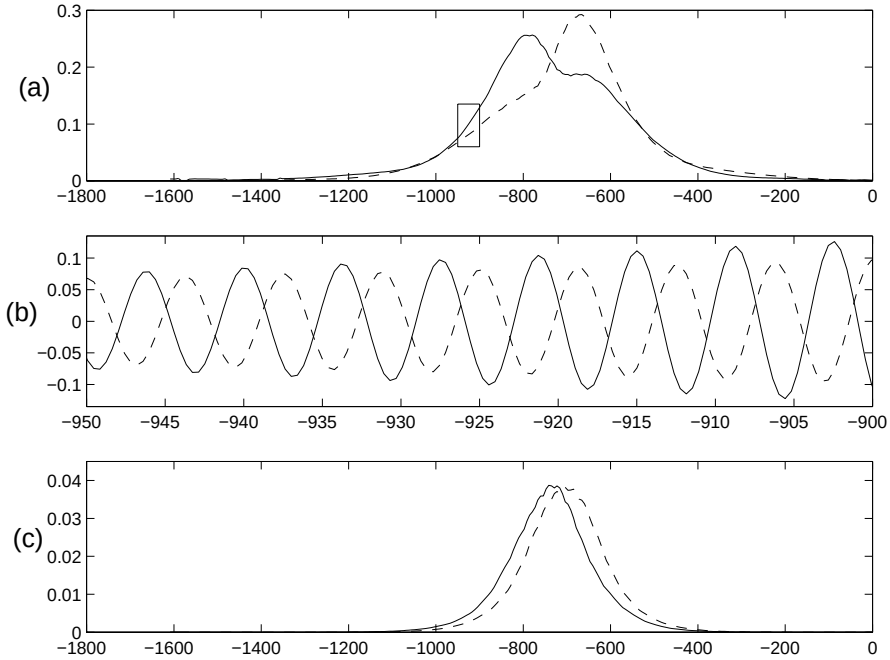

Fig. 12. The full (solid) and approximate (dashed) solution at $t = 12000$ for **(a)** the electric field envelope, **(b)** the full electric field, blown up from the box in (a), showing that the two solutions are out of phase, and **(c)** the energy density, which agrees quite well.

(ii) The very long time simulations described in Section 7 indicate a degradation of the gap soliton due to wave steepening and the radiation of energy away from the soliton core. It would be of interest to derive higher order model equations that describe these phenomena and agree with the full solutions to AMLE on longer timescales.

While it is possible to find longer-time envelope equations by starting with smaller ($\mathcal{O}(\varepsilon)$) initial conditions and introducing a third timescale $T_2 = \varepsilon^2 t$, our primary interest is to investigate the validity of the NLCME system already in wide use by experimentalists. Rigorous results for such longer-time systems in other contexts are given in [23], [31].

(iii) For the one-dimensional nondispersive model with nonlinearity, we have seen that wave steepening and shock formation occurs. This situation appears to persist in the presence of periodic structure. It would be of interest to extend the Lax-Klainerman-Majda theory [28] described in Section 3.4 to include the case of equations with periodic or more general inhomogeneous variable coefficient terms. As noted, for (localized) SVEA initial conditions with carrier frequency in Bragg resonance with the medium, photonic band dispersion is significantly stronger than material dispersion and the gap solitons arise due to a balance between the former and the Kerr nonlinearity (indeed, the NLCME may be obtained as a Galerkin truncation of the infinite system of equations (39)) derived in this case. Inclusion of material

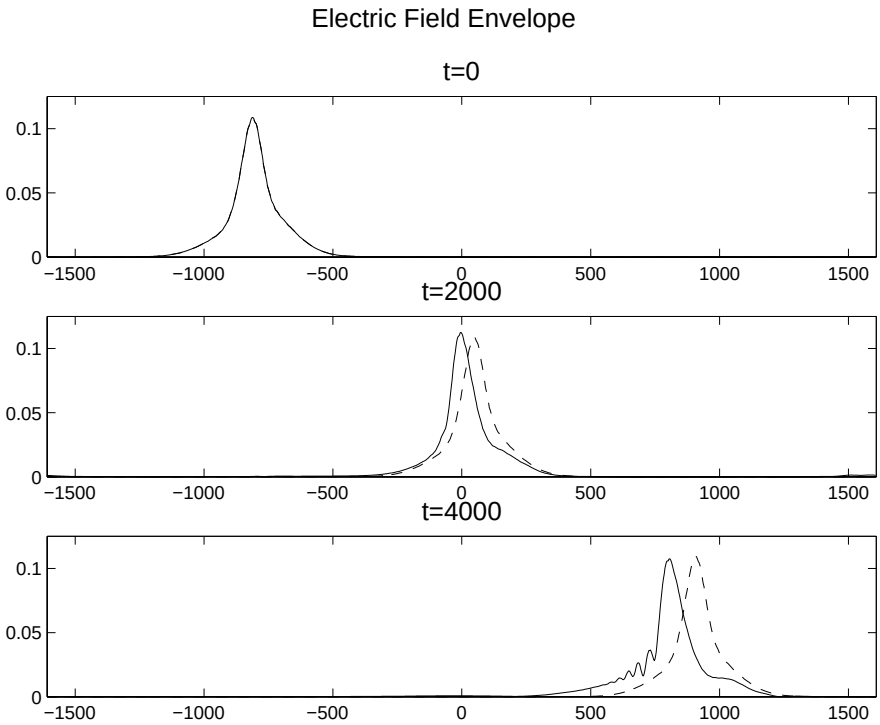

Fig. 13. The envelope of the solution with very few oscillations steepening and then breaking up.

dispersion ($\omega_0 < \infty$ in AMLE) regularizes shocks; see Theorem 3. Are there subtle regularizing effects provided by photonic band dispersion alone?

(iv) In the full three-dimensional waveguide problem, one must also take into account waveguide/mode dispersion and polarization mode dispersion. In this case there is an interplay between the mechanisms of diffractive spreading (regularizing), geometric confinement of the field (tending to one-dimensionalize and therefore singularize the propagation), modal dispersion (which takes higher harmonics off resonance and therefore possibly regularizes), and nonlinearity. The interplay of all these effects remains unclear. It would be interesting to extend the results of [12], [23], [31], [40], [39] to situations with periodicity and nontrivial transverse geometry.

A. Dimensionless Quantities

In this appendix, we nondimensionalize AMLE and isolate the key nondimensional parameters. We then define *dispersion lengths* and *nonlinear length* whose balance specifies the conditions under which a soliton is expected to form. Finally, using the experimental parameters of Eggleton et al. [15], we calculate our dimensionless quantities and verify the applicability of AMLE.

We begin with the AMLE system written using dimensional variables and derive a nondimensional version of AMLE. We then use physical parameter values gleaned from the literature in order to find approximate sizes of the nondimensional parameters. Primed variables represent nondimensional quantities and unprimed variables dimensional ones. We use the standard notation $[X]$ to represent the units of X so that $X = [X]X'$ for any variable X.

The AMLE written in dimensional variables are

$$\mu_0 \partial_t D = \partial_z B, \;\; \partial_t B = \partial_z E, \tag{121a}$$

$$D \equiv \epsilon_0 E + P, \tag{121b}$$

$$\tilde{\omega}_0^{-2} \partial_t^2 P + (1 - 2\Delta n \cos(2\tilde{k}_B z)) P - \tilde{\phi} P^3 = \epsilon_0 \chi^{(1)} E. \tag{121c}$$

We begin, as usual, by eliminating the magnetic field B to obtain

$$\mu_0 \partial_t^2 D = \partial_z^2 E. \tag{122}$$

We now introduce nondimensional (primed) variables,

$$t = \mathcal{T} t', \qquad z = \mathcal{Z} z', \tag{123a}$$

$$E = \mathcal{E} E', \qquad P = \epsilon_0 \mathcal{E} P', \qquad D = \epsilon_0 \mathcal{E} D', \tag{123b}$$

$$\tilde{k}_B = \frac{k_B}{\mathcal{Z}}, \qquad \tilde{\omega}_0 = \frac{\omega_0}{\mathcal{T}}, \tag{123c}$$

where the calligraphic letters represent dimensional magnitudes. To explicitly display the expected scaling, we write

$$\Delta n = \varepsilon \nu \quad \text{and} \quad \tilde{\phi} = \frac{\varepsilon \phi}{(\epsilon_0 \mathcal{E})^2}, \tag{124}$$

where ν and ϕ, along with $\chi^{(1)}$, are dimensionless and $\mathcal{O}(1)$, and the fields in (123b) are also all $\mathcal{O}(1)$.

Substituting these new variables into equations (122), (121b), and (121c) and eliminating common factors yields

$$\tfrac{\mu_0 \epsilon_0}{\mathcal{T}^2} \partial_{t'}^2 D' = \tfrac{1}{\mathcal{Z}^2} \partial_{z'}^2 E', \tag{125a}$$

$$D' = E' + P', \tag{125b}$$

$$\tfrac{1}{{\omega_0}^2} \partial_{t'}^2 P' + [1 + 2\varepsilon \nu \cos(2k_B z')] P' - \varepsilon \phi {P'}^3 = \chi^{(1)} E'. \tag{125c}$$

Letting

$$\mathcal{T} = \frac{\mathcal{Z}}{c}, \tag{126}$$

we have that (125a) becomes

$$\partial_{t'}^2 D' = \partial_{z'}^2 E'. \tag{127}$$

The system (127), (125b), and (125c) comprise the dimensionless AMLE system; see also (6).

A.1. The Material Frequency $\tilde{\omega}_0$ and the Electric Susceptibility $\chi^{(1)}$

At low intensities, the relation between P and E is given by the *Lorentz* model:

$$\frac{1}{\tilde{\omega}_0^2} P_{tt} + P = \epsilon_0 \chi^{(1)} E. \tag{128}$$

In the time-frequency domain, this implies

$$\hat{P}(\omega) = \epsilon_0 \frac{\tilde{\omega}_0^2}{\tilde{\omega}_0^2 - \omega^2} \hat{E}(\omega), \tag{129}$$

where $\hat{f}(\omega) = \int e^{-i\omega t} f(t)\, dt$.

In a general linear setting, we have

$$\hat{P}(\omega) = \chi^{(1)}(\omega) \hat{E}, \tag{130}$$

where the (frequency dependent) index of refraction, $n(\omega)$, is related to $\chi^{(1)}$ by the relation

$$n^2(\omega) \;=\; 1 + \chi^{(1)}(\omega). \tag{131}$$

A standard model for $\chi^{(1)}(\omega)$ in the optics literature [2] is the Sellmeier model, which approximates $\chi^{(1)}(\omega)$ by a function of the form

$$\chi^{(1)}(\omega) = \epsilon_0 \sum_{i=1}^{N} \frac{\omega_i^2 \chi_i^{(1)}}{\omega_i^2 - \omega^2}, \tag{132}$$

where ω_i, the model resonant frequencies of the medium, and $\chi_i^{(1)}$ are determined by a data fit. For silica glass, a good fit with experimental data is found with $N = 3$. The Lorentz model corresponds to $N = 1$, so we take the term in the $N = 3$ expansion corresponding to that frequency, ω_i, which is closest to the input carrier frequency. Below, we use this to determine the values of $\tilde{\omega}_0$ and $\chi^{(1)}$ in the Lorentz model.

A.2. The Electric Field Strength $\mathcal{E}$

Most optical physics literature reports field strength in terms of the intensity, I. The electric field strength is given in terms of the intensity by [2]:

$$\mathcal{E}^2 = \frac{2I}{\epsilon_0 c n}, \tag{133}$$

where n is the (nondimensional) refractive index, related to the linear susceptibility, $\chi^{(1)}$, by (131).

A.3. The Coefficient of Nonlinearity, $\tilde{\phi}$

We consider the instantaneous limit of the basic equation, with no grating, i.e., $\Delta n = 0$:

$$P - \tilde{\phi} P^3 = \epsilon_0 \chi^{(1)} E. \tag{134}$$

We may invert the above relation for small E and write

$$P = \epsilon_0 \left(\chi^{(1)} E + \chi^{(3)} E^3 + \cdots \right), \tag{135}$$

where

$$\tilde{\phi} = \frac{\chi^{(3)}}{\epsilon_0^2 \chi^{(1)^3}}. \tag{136}$$

Then the nondimensional quantity is given by

$$\varepsilon\phi = \frac{\mathcal{E}^2 \chi^{(3)}}{(\chi^{(1)})^3}. \tag{137}$$

The third-order susceptibility $\chi^{(3)}$ is related to the nonlinear refractive index, n_2 or n_2^I, by the relation ([2], page 40, equation (2.3.13) and page 582, equation (B.2)):

$$\chi^{(3)} = \frac{8nn_2}{3} = \frac{4\epsilon_0 c n^2 n_2^I}{3}. \tag{138}$$

Finally, since $I = \frac{1}{2}\epsilon_0 c n \mathcal{E}^2$ ([2], page 582, equation (B.1)), we have

$$\varepsilon\phi = \frac{8Inn_2^I}{3(\chi^{(1)})^3}. \tag{139}$$

A.4. Parameter Values of Physical Experiments

To form the anharmonic oscillator equation for the polarization, we need four constants: the susceptibility $\chi^{(1)}$, the nondimensional frequency ω_0, the index modulation Δn, and the cubic coefficient ϕ.

The Susceptibility $\chi^{(1)}$ and the Nondimensional Frequency ω_0

First we must find the characteristic timescale $\mathcal{T}$. Typical experiments are performed using laser light with wavelength of approximately one micron. We define the characteristic length and time so that $k_B \approx 1$, but for convenience in the paper refer to k_B. Accordingly, we take

$$\mathcal{Z} = \frac{1 \times 10^{-6}}{2\pi}\text{m} \approx 1.6 \times 10^{-7}\text{m}, \tag{140}$$

$$\mathcal{T} = \frac{\mathcal{Z}}{c} \approx 5.3 \times 10^{-16}\text{s}. \tag{141}$$

Next, we must find the dimensional frequency of the oscillator. For silica glass, one has ([2], page 7)

$$\tilde{\omega}_0 = 1.6 \times 10^{16}\text{s}^{-1}, \tag{142}$$

$$\chi^{(1)} = .41. \tag{143}$$

The nondimensional resonant frequency is then given by

$$\omega_0 = \tilde{\omega}_0 \mathcal{T} \approx 8.6. \tag{144}$$

The Index Modulation $\Delta n = \varepsilon\nu$
Eggleton et al. [15] give an approximate value of

$$\Delta n \approx 3 \times 10^{-4}. \tag{145}$$

The Nondimensional Nonlinearity Coefficient, ϕ
For this we need the intensity, which in [13] is given by

$$I \approx 2 \times 10^{14}\ \mathrm{W/m^2}, \tag{146}$$

and the nonlinear refractive index ([2], pages 582–583),

$$n_2^I = 2.5 \times 10^{-20}\ \mathrm{m^2/W}. \tag{147}$$

The linear refractive index is obtained from (131) and (143):

$$n \approx 1.2. \tag{148}$$

From (139), we have

$$\varepsilon\phi \approx 2 \times 10^{-4}. \tag{149}$$

Therefore, by choosing the small parameter

$$\varepsilon = 10^{-4}, \tag{150}$$

we arrive at

$$\phi \approx 2 \tag{151}$$

and

$$\nu \approx 3. \tag{152}$$

Therefore, the approximate nondimensional polarization equation (125c) may be written:

$$\mathcal{O}(10^{-2})\partial_{t'}^2 P' + [1 + \mathcal{O}(10^{-4})\cos(2k_B z')]P' + \mathcal{O}(10^{-4})P'^3 = \mathcal{O}(1)E'. \tag{153}$$

We see that the nonlinearity and the dimensionless grating effectively balance each other. This justifies our ε-dependent scaling of the dimensionless AMLE system and the solution. We note that this scaling assumes that E', P', and D' are $\mathcal{O}(1)$ quantities; see (123b). In the main text, we take E, P, and D to be $\mathcal{O}(\sqrt{\varepsilon})$, thereby effectively introducing the factor of ε multiplying ϕ in (125c) which is absent from (6c).

Note also, that while ${\omega_0}^{-2}$, the coefficient of $\partial_{t'}^2 P'$, is small, it is roughly 100 times the grating strength, i.e., $\varepsilon\omega_0^2 \sim 10^{-2}$. The significance of this can be seen as follows. Were we to expand the electric field, as in Section 4, to all orders in ε, we would have

$$E \approx \sqrt{\varepsilon}\sum_{i=0}^{\infty}\varepsilon^i E_i.$$

Inspection of the hierarchy of equations for E_i reveals that

$$E_i \sim {\omega_0}^{2i}.$$

This suggests that E^ε is well approximated by $\varepsilon^{\frac{1}{2}}E_0$ provided $\varepsilon{\omega_0}^2 \ll 1$. The experimental regime discussed satisfies this criterion.

B. Calculation of the Dispersion and Nonlinear Lengths

In the design of an experiment to observe gap solitons, the matter of the *formation length* is important. Laser light injected into an optical fiber will have an approximately Gaussian profile. One is therefore interested in the distance over which one can expect a soliton to form. Solitons are understood to form due to a balance of dispersive and nonlinear effects. Dispersion acts by broadening a pulse and radiating high frequency components away, while a Kerr (focusing) nonlinearity acts to concentrate energy. We presently give a heuristic discussion of this balance.

Material Dispersion Length, $z_{\mathrm{D,material}}$

Recall that the (material) dispersion relation associated with the finite time response of the medium to the field is

$$k^2 = \omega^2 \frac{n^2 - \left(\frac{\omega}{\omega_0}\right)^2}{1 - \left(\frac{\omega}{\omega_0}\right)^2}. \tag{154}$$

The dispersion of a wavepacket, with frequency content concentrated in an interval of width ε about ω_B, is governed by Fourier integrals of the form

$$I(z,t) = \int e^{i(k(\omega)z' - \omega t')} f\left(\frac{\omega - \omega_B}{\varepsilon}\right) d\omega, \tag{155}$$

where f is a localized function of frequency. Expansion of $k(\omega)$ about $\omega = \omega_B$ yields

$$\begin{aligned} I(z',t') &\sim e^{i(k_B z' - \omega_B t')} \int e^{i(\omega-\omega_0)(k'(\omega_B)z' - \omega_B t')} e^{i\frac{k''(\omega_B)}{2}(\omega-\omega_B)^2 t'} f\left(\frac{\omega-\omega_B}{\varepsilon}\right) d\omega \\ &\sim \varepsilon e^{i(k_B z' - \omega_B t')} \int e^{i\mu(k'(\omega_B)(\varepsilon z') - \omega_B(\varepsilon t'))} e^{i\frac{k''(\omega_B)}{2}\mu^2(\varepsilon^2 z')} f(\mu)\, d\mu \\ &= \mathcal{O}((k''(\omega_B)\varepsilon^2 z')^{-\frac{1}{2}}), \qquad z' = \mathcal{O}(\varepsilon^{-2}). \end{aligned} \tag{156}$$

Thus, a localized pulse disperses due to the finite time response of the medium over a dimensionless distance z' of order $\varepsilon^{-2}k''(\omega_B)^{-1}$. Noting that $k''(\omega_B) = \mathcal{O}(\omega_0^{-2})$, we have

$$z_{\mathrm{D,material}} = \mathcal{O}(\varepsilon^{-2}k''(\omega_B)^{-1}) = \mathcal{O}(\omega_0^2\varepsilon^{-2}) \text{ wavelengths.}$$

Using the physical parameter values discussed in Appendix A, we find that

$$z_{\mathrm{D,material}} \approx 7 \text{ km.}$$

Photonic Band Dispersion Length, $z_{\mathrm{D,band}}$

Linear dispersion due to the periodic structure (photonic band dispersion) is governed by the linear coupled mode equations (27). The dispersion of the wave envelope is then

expressed in terms of generalized Fourier superpositions of Floquet-Bloch waves:

$$\begin{aligned} I(z',t') &\sim \int E(z',t',;k_B+\varepsilon Q)\,f(Q)\,dQ \\ &\sim e^{i(k_B z'-\omega_B t')}\,e^{-i\Omega(0)\varepsilon t'}\int e^{iQ(\varepsilon z'-\Omega'(0)\varepsilon t')}\,e^{-\frac{i}{2}\Omega''(0)Q^2\varepsilon t'}\,f(Q)\,dQ \\ &= \mathcal{O}((\Omega''(0)\varepsilon t)^{-\frac{1}{2}}), \qquad t'=\mathcal{O}(\varepsilon^{-1}), \end{aligned} \tag{157}$$

where $\Omega(Q)$ is given by the dispersion relation (29) which disperses to zero over a distance

$$z_{\mathrm{D,band}} = \mathcal{O}([\varepsilon\Omega''(0)]^{-1}) = \mathcal{O}\left(\frac{\kappa}{\varepsilon}\right) \text{wavelengths.}$$

Physically, this gives

$$z_{\mathrm{D,band}} \approx 1 \text{ cm},$$

which is six orders of magnitude shorter than $z_{\mathrm{D,material}}$.

Nonlinear Length, z_{NL}

A measure of the distance z_{NL}, over which nonlinear effects play a role, can be obtained by considering the coupled mode equations in the absence of dispersion. If E_0 denotes the electric field amplitude, then we have

$$(\partial_T \pm v_g\partial_Z)E = -i\Gamma|E|^2E, \tag{158}$$

with solution $E = e^{-i\Gamma\mathcal{E}^2(Z-v_gT)}\mathcal{E} = e^{-i\Gamma\mathcal{E}^2(\varepsilon z'-v_g\varepsilon t')}\mathcal{E}$, for some constant $\mathcal{E}$. Therefore,

$$z_{\mathrm{NL}} = (\varepsilon\Gamma)^{-1} \sim (\varepsilon\phi)^{-1} \text{ wavelengths},$$

which gives

$$z_{\mathrm{NL}} \approx 1 \text{ cm},$$

which balances the band dispersion length $z_{\mathrm{D,band}}$.

Balance of Nonlinearity and Dispersion

Note that $z_{\mathrm{D,material}}$ is longer than $z_{\mathrm{D,band}}$ by a factor of order ε^{-1}; for frequencies near the band edge, the dispersion due to the periodic structure is much stronger than material dispersion.

Therefore, in order to achieve a balance between dispersive and nonlinear effects over a short distance, we must equate $z_{\mathrm{D,band}}$ and z_{NL}. This gives

$$\frac{\kappa}{\varepsilon} \sim \frac{1}{\phi} \quad \text{or} \quad \kappa\phi \sim \varepsilon. \tag{159}$$

By (139), this gives the intensity, ensuring a balance of appearance of nonlinear effects within a (photonic band) dispersion length, $z_{\mathrm{D,band}}$,

$$I \sim \frac{3}{8}\frac{(\chi^{(1)})^3\varepsilon}{nn_2^I\kappa},$$

which works out to

$$I = \mathcal{O}(10^{14}) \text{ W/m}^2,$$

in line with the experiments described in [13].

C. Computational Details

C.1. Computations in Sections 3.4 and 3.5

All figures in these sections are initialized as a single normal mode of wavenumber $k = 1$ of the linearized form of the AMLE, 6, with $\nu = 0$ and magnitude $\sqrt{\varepsilon}$. We should note that the numerical simulations use very large values of ε compared to the physically appropriate value $\varepsilon = \mathcal{O}(10^{-4})$ derived in Appendix A because performing the simulations for AMLE with such small ε would be computationally infeasible. The other parameters are given by

$$n^2 - 1 = 1 \quad \text{and} \quad \phi = 1.$$

For Figure 4, we use a frequency of $\omega_0 = 1000$ to illustrate the behavior near the limit of instantaneous polarization before the onset of a shock. In Figures 5 and 6, we use $\omega_0 = 50$ and $\omega_0 = 100$, respectively, to show the role of dispersion in regularizing the shock.

C.2. Computations in Section 7

All calculations in this section are performed with the following parameter values:

$$\begin{aligned} \varepsilon &= \frac{1}{32}, \\ k_B &= 1, \\ n &= 1.19, \\ \phi &= 1, \\ \nu &= 1. \end{aligned}$$

In Figures 7, 9, and 12, a material frequency of

$$\omega_0 = 4$$

is used, while in Figure 13, we use the value

$$\omega_0 = 1.$$

In all calculations, the coefficients of the NLCME are derived from the above parameters, and, as initial conditions, we construct a solution from the gap soliton with parameters

$$v = .9 \quad \text{and} \quad \delta = .9.$$

To create the graphs in Figures 10 and 11, we also compute the evolutions with all parameters as above except with $\varepsilon = \frac{1}{64}$.

Acknowledgments

R. H. Goodman was supported by an NSF University-Industry postdoctoral fellowship DMS-99-01897. P. J. Holmes was partially supported by DOE grant DE-FG02-95ER25238. The authors wish to acknowledge informative and stimulating conversations with the following individuals: Alejandro Aceves, Ben Eggleton, Dick Slusher, Gadi Lenz, Mel Lax, Eduard Kirr, Stefan Spalter, Peter Oswald, Steve Golowich, and an anonymous referee who pointed out numerous relevant references.

References

1. A. B. Aceves and S. Wabnitz, *Self-induced transparency solitons in nonlinear refractive periodic media*, Phys. Lett. A **141** (1989), 37–42.
2. G. P. Agrawal, *Nonlinear fiber optics*, 2nd ed., Academic Press, San Diego, 1995.
3. N. Aközbek and S. John, *Optical solitary waves in two and three-dimensional nonlinear photonic band-gap structures*, Phys. Rev. E **57** (1998), 2287–2319.
4. A. Babin and A. Figotin, *Nonlinear photonic crystals I: Quadratic nonlinearity*, preprint (2000).
5. R. W. Boyd, *Nonlinear optics*, Academic Press, New York, 1992.
6. N. G. R Broderick, D. Taverner, D. J. Richardson, M. Ibsen, and R. I. Laming, *Experimental observation of nonlinear pulse compression in nonuniform Bragg gratings*, Opt. Lett. **22** (1997), no. 24, 1837–1839.
7. T. G. Brown and B. J. Eggleton, *Focus issue: Bragg solitons and nonlinear optics of periodic structures*, Optics Express (1998), Vol. 3, no. 11.
8. W. Chen and D. L. Mills, *Gap solitons and the nonlinear optical response of superlattices*, Phys. Rev. Lett. **58** (1987), 160–163.
9. D. N. Christodoulides and R. I. Joseph, *Slow Bragg solitons in nonlinear periodic structures*, Phys. Rev. Lett. **62** (1989), 1746–1749.
10. C. M. de Sterke and J. E. Sipe, *Envelope-function approach for the electrodynamics of nonlinear periodic structures*, Phys. Rev. A **38** (1988), 5149–5165.
11. C. M. de Sterke and J. E. Sipe, *Gap solitons*, Prog. Opt. **33** (1994), 203–260.
12. P. Donnat and J. Rauch, *Dispersive nonlinear geometric optics*, J. Math. Phys. **38** (1997), 1484–1523.
13. B. J. Eggleton, C. M. de Sterke, and R. E. Slusher, *Nonlinear pulse propagation in Bragg gratings*, J. Opt. Soc. Am. B **14** (1997), no. 11, 2980–2992.
14. B. J. Eggleton, C. M. de Sterke, and R. E. Slusher, *Bragg solitons in the nonlinear Schrödinger limit: Experiment and theory*, J. Opt. Soc. Am. B **16** (1999), no. 4, 587–599.
15. B. J. Eggleton, R. E. Slusher, C. M. de Sterke, P. A. Krug, and J. E. Sipe, *Bragg grating solitons*, Phys. Rev. Lett. **76** (1996), no. 10, 1627–1630.
16. R. G. Flesch, A. Pushkarev, and J. V. Moloney, *Carrier wave shocking of femtosecond optical pulses*, Phys. Rev. Lett. **76** (1996), no. 14, 2488–2491.
17. T. Opatrny G. Kurizki, A. E. Kozhekin, and B. Malomed, *Optical solitons in periodic media with resonant and off-resonant nonlinearities*, Prog. Opt., to appear.
18. C. S. Gardner, J. M. Greene, M. D. Kruskal, and R. M. Miura, *Method for solving the Korteweg-de Vries equation*, Phys. Rev. Lett. **19** (1967), 1095–1097.
19. L. Gilles, J. V. Moloney, and L. Vázquez, *Electromagnetic shocks on the optical cycle of ultrashort pulses in triple-resonance Lorentz dielectric media with subfemtosecond nonlinear electronic Debye relaxation*, Phys. Rev. E **60** (1999), 1051–1059.
20. D. Gottlieb and S. A. Orszag, *Numerical analysis of spectral methods: Theory and applications*, Society for Industrial and Applied Mathematics, Philadelphia, Pa., 1977, CBMS-NSF Regional Conference Series in Applied Mathematics, No. 26.

21. A. Iserles, *A first course in the numerical analysis of differential equations*, Cambridge University Press, Cambridge, 1996.
22. F. John, *Partial differential equations*, fourth ed., Springer-Verlag, New York, 1991.
23. J. Joly, G. Metivier, and J. Rauch, *Diffractive nonlinear geometric optics with rectification*, Indiana Univ. Math. J. **47** (1998), 1167–1241.
24. J. L. Joly, G. Metivier, and J. Rauch, *Global solvability of the anharmonic oscillator model from nonlinear optics*, SIAM J. Math. Anal. **27** (1996), no. 4, 905–913.
25. R. Kashyap, *Fiber Bragg gratings*, Academic Press, San Diego, 1999.
26. T. Kato, *The Cauchy problem for the Korteweg-de Vries equation*, Nonlinear partial differential equations and their applications. Collège de France Seminar, Vol. I (Paris, 1978/1979), Pitman, Boston, 1981, pp. 293–307.
27. P. Kirrmann, G. Schneider, and A. Mielke, *The validity of modulation equations for extended systems with cubic nonlinearities*, Proc. Roy. Soc. Edinburgh **122A** (1992), 85–91.
28. S. Klainerman and A. Majda, *Formation of singularities for wave equations including the nonlinear vibrating string*, Commun. Pure Appl. Math. **33** (1980), no. 3, 241–263.
29. H. Kogelnik, *Coupled wave theory for thick holograms*, Bell Syst. Tech. J. **48** (1969), no. 9, 2909–2947.
30. E. Korotyaev, *The propagation of waves in periodic media at large time*, Asymptot. Anal. **15** (1997), 1–24.
31. D. Lannes, *Dispersive effects for nonlinear geometrical optics with rectification*, Asymptot. Anal. **18** (1998), 111–146.
32. P. D. Lax, *Hyperbolic systems of conservation laws and the mathematical theory of shock waves*, Society for Industrial and Applied Mathematics, Philadelphia, 1973, Conference Board of the Mathematical Sciences Regional Conference Series in Applied Mathematics, No. 11.
33. P. D. Lax and C. D. Levermore, *The small dispersion limit of the Korteweg-de Vries equation I*, Commun. Pure Appl. Math. **36** (1983), no. 3, 253–290.
34. P. Millar, R. M. De la Rue, T. F. Krauss, J. S Aitchison, N. G. R. Broderick, and D. J. Richardson, *Nonlinear propagation effects in an AlGaAs Bragg grating filter*, Opt. Lett. **24** (1999), no. 10, 685–687.
35. A. C. Newell and J. V. Moloney, *Nonlinear optics*, Addison-Wesley Publishing Company Advanced Book Program, Redwood City, CA, 1992.
36. A. Owyoung, *The origins of the nonlinear refractive indices of liquids and glasses*, Ph.D. thesis, California Institute of Technology, 1971.
37. R. D. Pierce and C. E. Wayne, *On the validity of mean-field amptitude equations for counter-propagating wavetrains*, Nonlinearity **8** (1995), 769–779.
38. M. Reed, *Abstract nonlinear wave equations*, Springer-Verlag, Berlin–Heidelberg–New York, 1976, Lecture Notes in Mathematics, No. 507.
39. S. Schochet, *Fast singular limits of hyperbolic PDEs*, J. Diff. Eq. **114** (1994), 476–512.
40. S. Schochet, *Resonant nonlinear geometric optics for weak solutions of conservation laws*, J. Diff. Eq. **113** (1994), 473–504.
41. A. van Harten, *On the validity of the Ginzburg-Landau equation*, J. Nonlinear Sci. **1** (1991), 397–422.
42. S. Venakides, *The zero dispersion limit of the Korteweg-de Vries equation for initial potentials with nontrivial reflection coefficient*, Commun. Pure Appl. Math. **38** (1985), no. 2, 125–155.
43. G. B. Whitham, *Linear and nonlinear waves*, Wiley-Interscience [John Wiley & Sons], New York, 1974, Pure and Applied Mathematics.
44. H. G. Winful and G. D. Cooperman, *Self-pulsing and chaos in distributed feedback bistable optical devices*, Appl. Phys. Lett. **40** (1982), 298–300.
45. H. G. Winful, J. H. Marburger, and E. Garmire, *Theory of bistability in nonlinear distributed feedback structures*, Appl. Phys. Lett. **35** (1979), 379–381.
46. J. X. Xin, *Modeling light bullets with the two-dimensional sine-Gordon equation*, Physica D **135** (2000), no. 3–4, 345–368.
47. E. Yablonovitch, *Photonic band-gap structures*, J. Opt. Sci. Am. B **10** (1993), 283–295.